.

Ocean and Climate

1. Modern equilibrium: surface heat and water conditions

2. Decadal natural variability

   climate "noise" in time series but with characteristic spatial patterns ($e.g.$, ENSO), identified by Empirical Orthogonal Functions (EOFs)

3. Paleoclimate

   climate variations by solar brightening, volcanic cycles, atmospheric compositional changes, "snowball Earth", and Milankovich insolation cycles

4. Anthropogenic global change

   climate forcings by human pollution, land use, overfishing, and habitat destruction: warming, ice melt, sea level rise, stratification increase, acidification, deoxigenation, species extinction, and — probably, but not yet well identified — wind and circulation changes

Modern "Equilibrium": Sea Surface Temperature

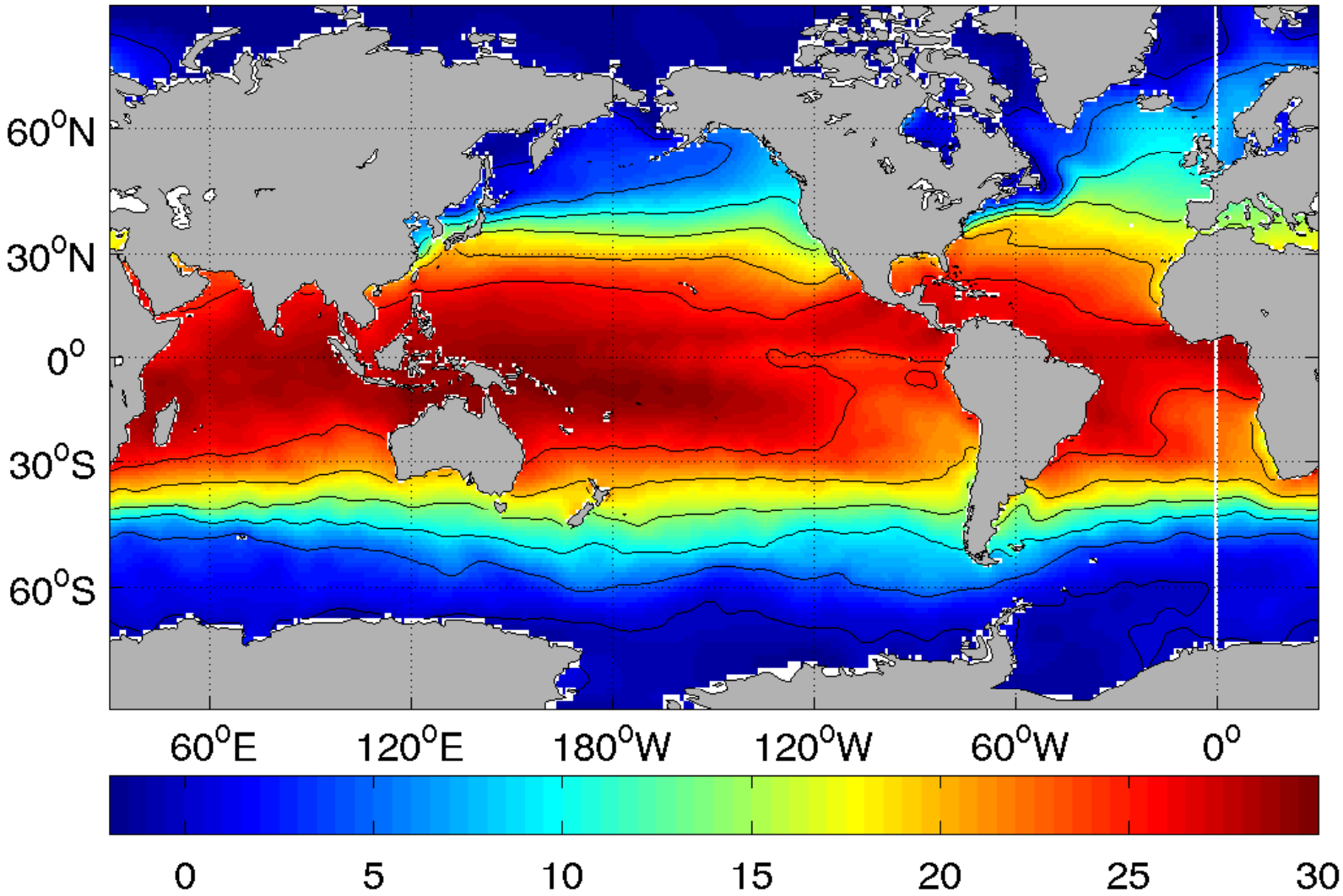

Annual mean temperature at the ocean surface (World Ocean Atlas, 2005). (repeated figure)

The present "equilibrium climate" is determined primarily from oceanic sea level, surface conditions, heat content, air-sea fluxes, and large-scale oceanic lateral transports of heat, salt, CO_2, *etc.*

The ocean-climate question is how these properties change as climate changes.

Sea Surface Salinity

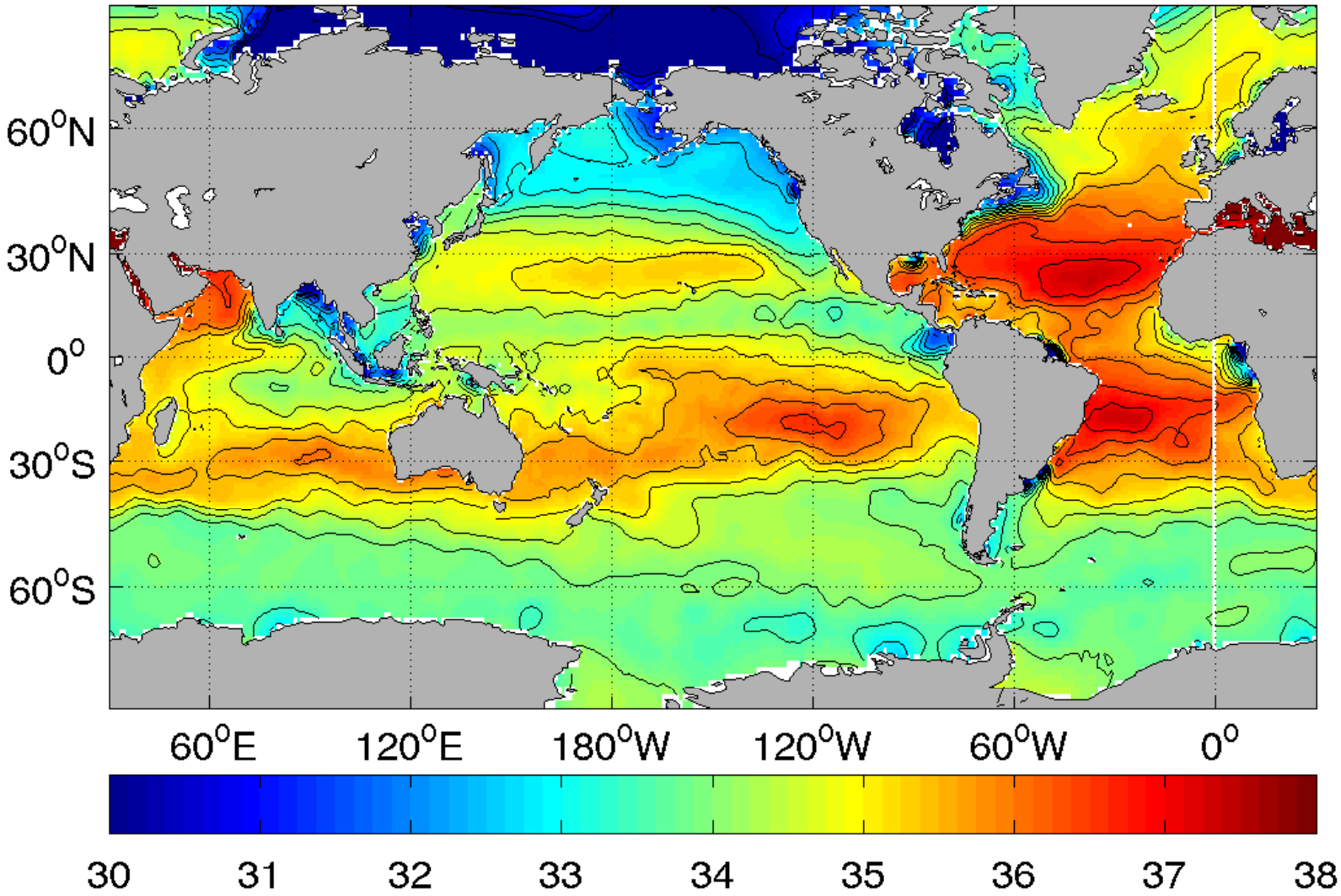

Annual mean salinity at the ocean surface (World Ocean Atlas, 2005). (repeated figure)

Mixed Layer Depth

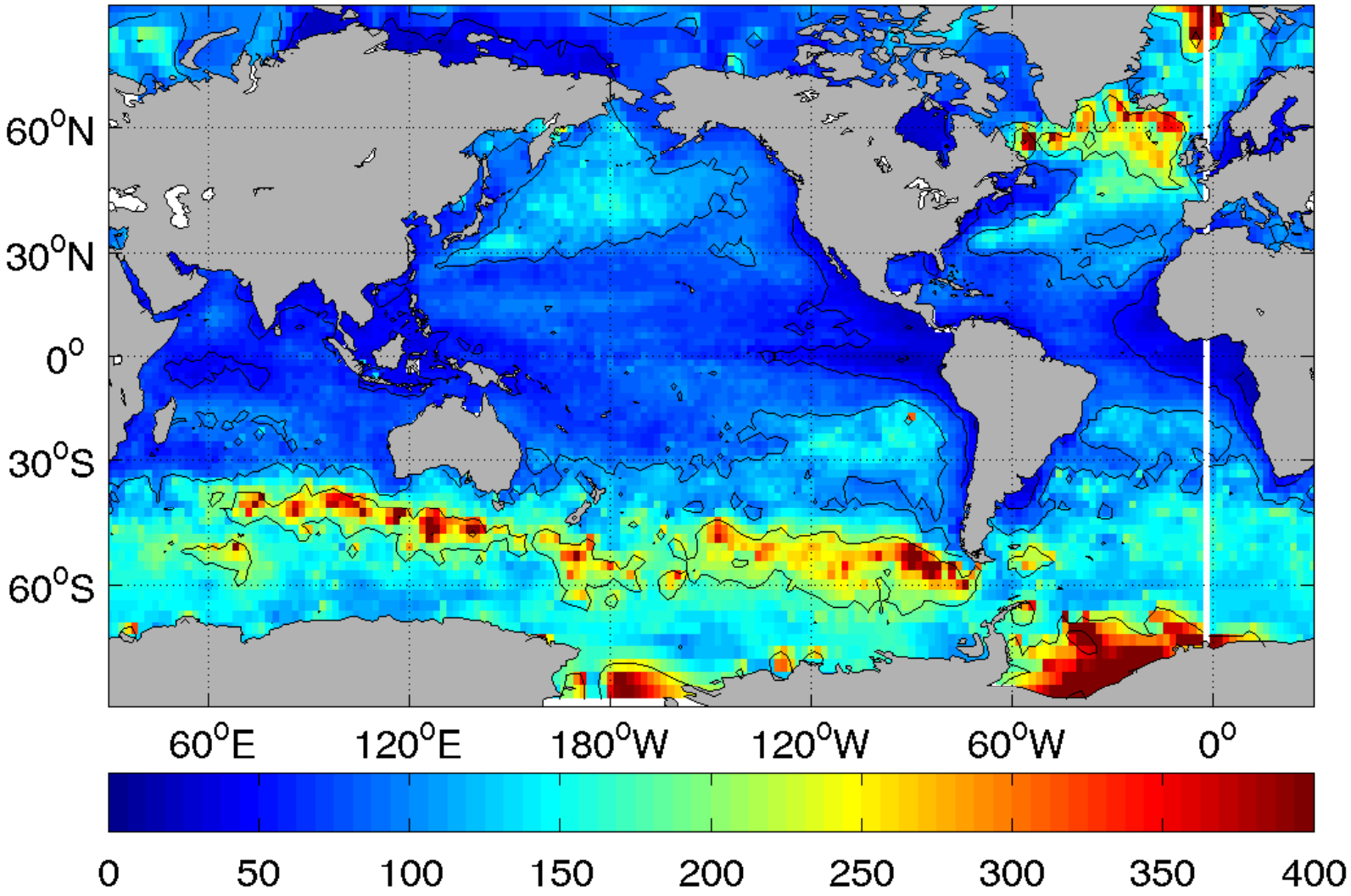

Maximum monthly mean depth [m] of the mixed layer, estimated from climatological profiles of T and S. (repeated figure; de Boyer *et al.*, 2004)

Surface Heat Flux

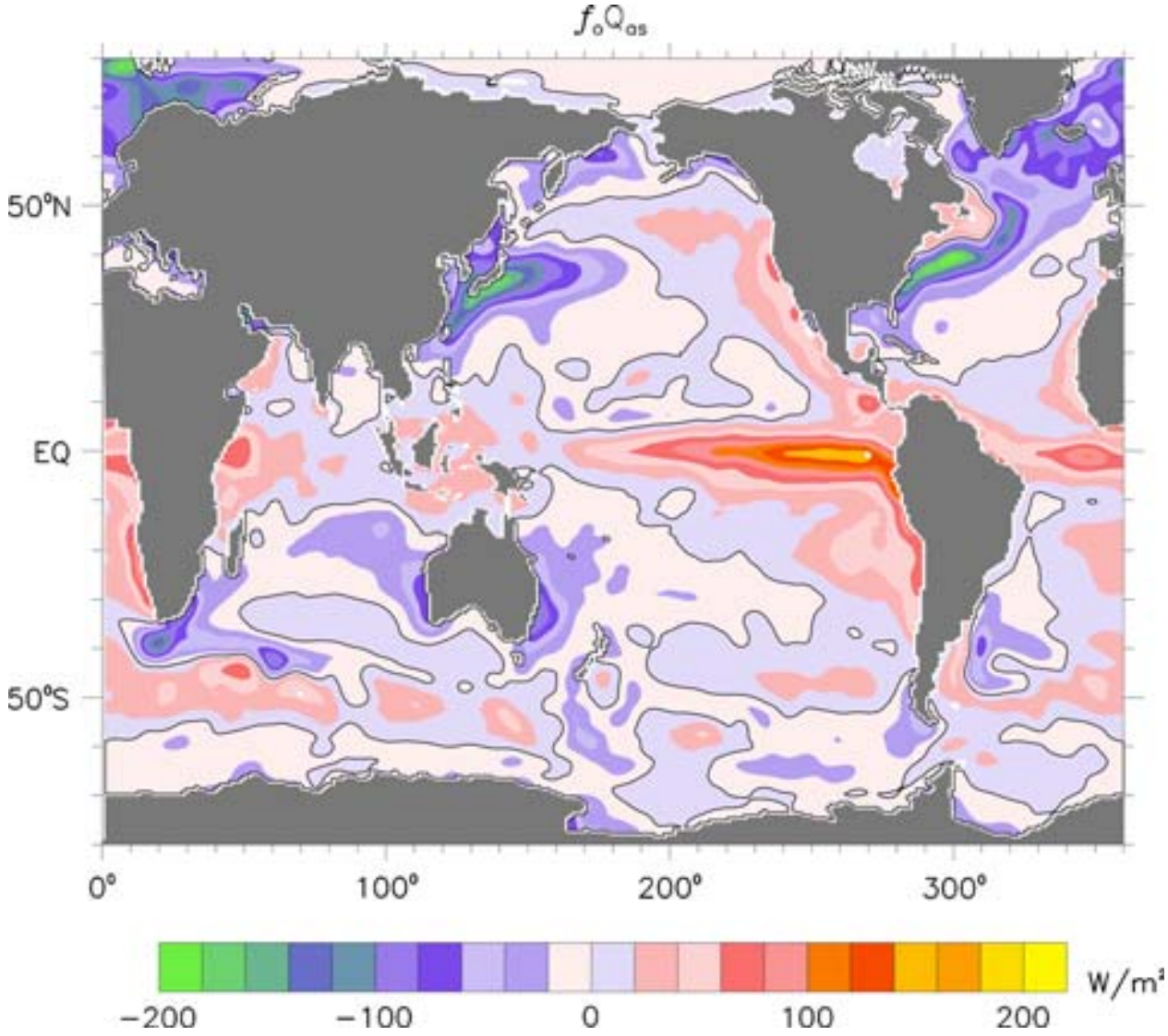

Mean surface heat flux, positive into the ocean. Colored at 20 W m^{-2} intervals. (repeated figure; Large and Yeagar, 2009)

Surface Fresh Water Flux

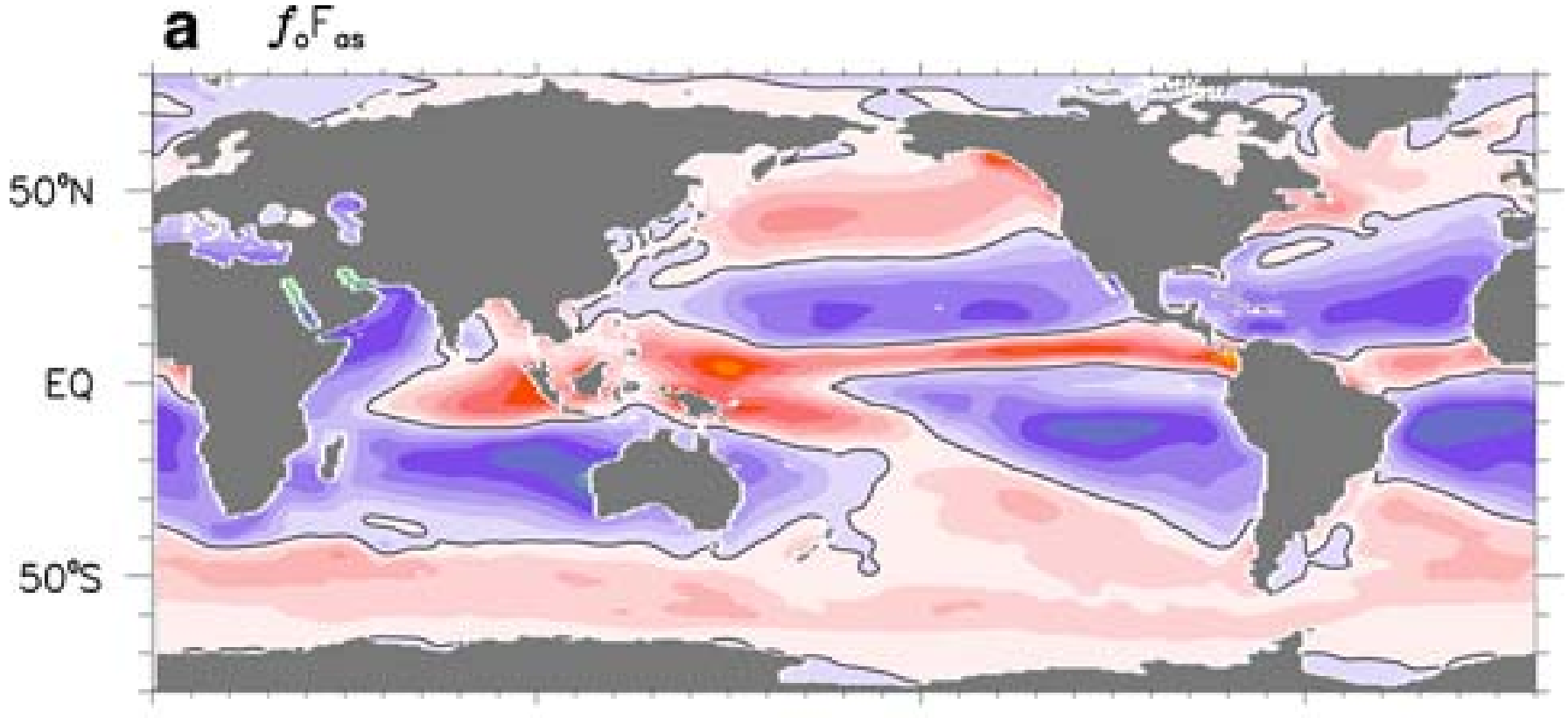

Mean surface water flux, positive into the ocean, and colored at 10 mg m/2 s^{-1} intervals. (repeated figure; Large and Yeagar, 2009)

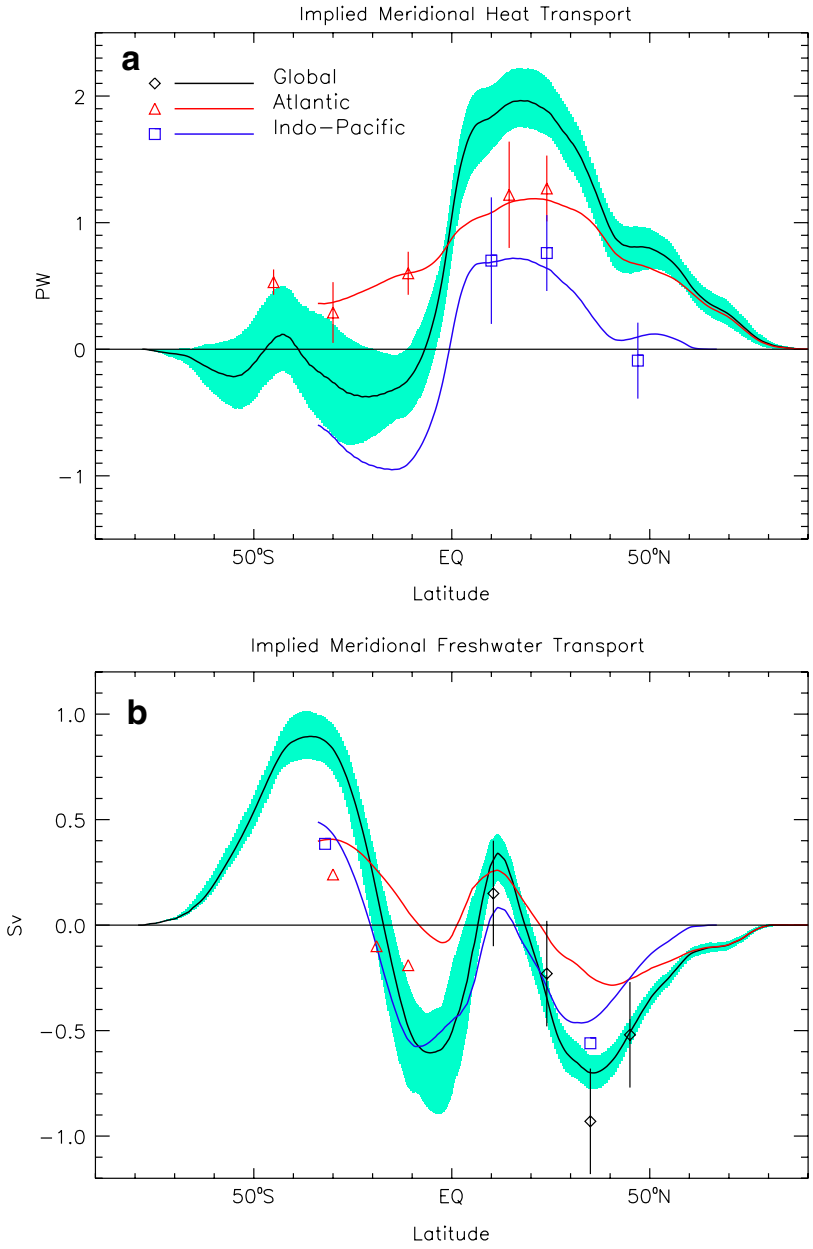

Northward ocean transports of (a) heat in PW and (b) freshwater in Sv. Curves are diagnosed from surface fluxes; points are *in situ* estimates. (Large and Yeagar, 2009)

Heat balance for zonal and depth integrated heat content:

$$\frac{d}{dt}\,\rho_0 C_p \int_{x_w}^{x_e}\int_{-h}^{0} dx\,dz\,T \;=\; -\,\partial_y \mathcal{H} + \int_{x_w}^{x_e} dx\,Q\,,$$

where $\mathcal{H}$ is the meridional oceanic heat flux by currents. In equilibrium, $\mathcal{H}$ is diagnosed from Q.
An analogous relation occurs for the integrated freshwater content.

(repeated figure)

Decadal Natural Variability

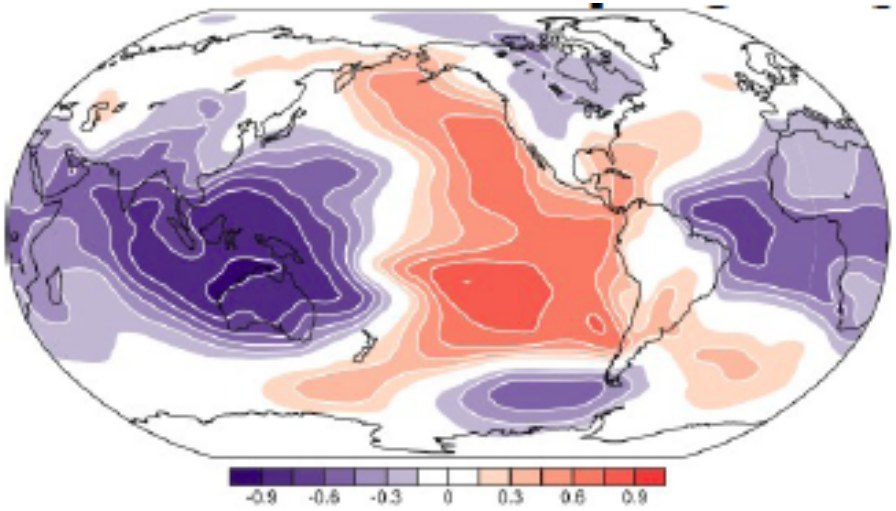

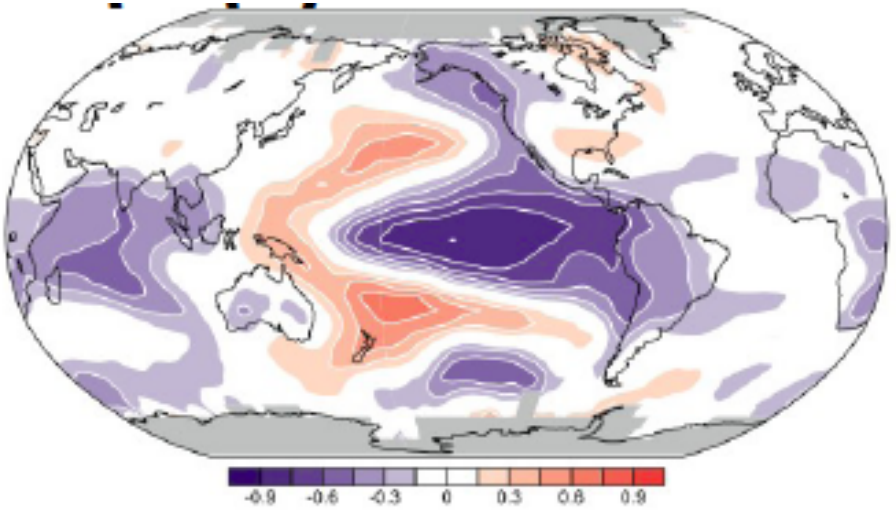

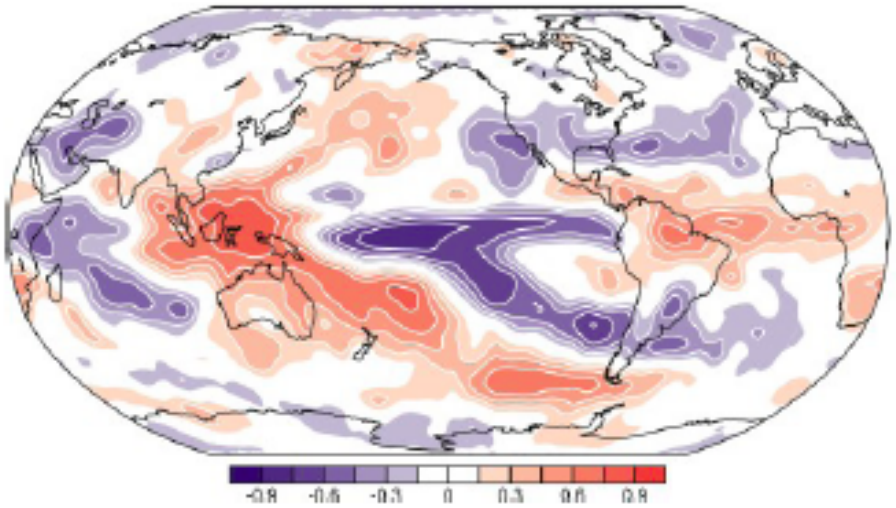

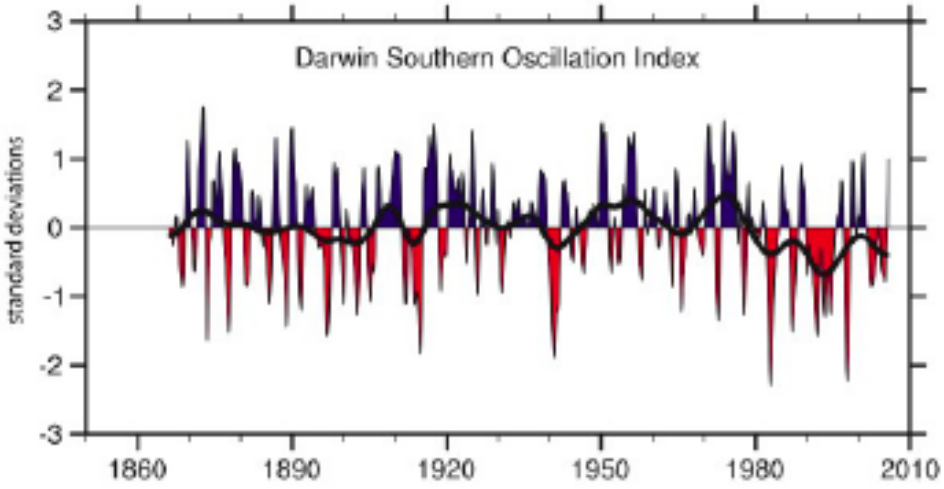

Correlations with the Southern Oscillation Index (Δp_{atm} between Tahiti and Darwin) in p_{atm}, SST, and precipitation. Also known as ENSO. The time series appears chaotic with a broad spectrum peak between 2-8 y in period. The spatial patterns are large-scale and roughly similar between events. This and other decadal modes are evident in both atmospheric and oceanic measurements.

Concept: All natural fluids with high Re exhibit spontaneous intrinsic variability, which tends to have red frequency and wavenumber spectra.

Because the ocean has a generally slower evolution than the atmosphere, $e.g.$, with an advective time scale $\sim \ell/V$, its spectra are redder.

To the extent that atmospheric and oceanic intrinsic variability are coupled — which should be the default perspective until proven otherwise — the oceanic coupling will act to redden the atmospheric spectrum.

The ocean affects the atmosphere primarily in three ways:

- SST provides a thermal reservoir for the atmosphere and imposes gradients in surface wind through modulation of the atmospheric boundary layer stability: warm water induces a less stable layer.

- Oceanic currents modulate the surface stress that depends on the relative difference between surface wind and current: this generally reduces stress, extracts eddy energy from the ocean, and energizes surface winds.

- Seaice has a much larger albedo than seawater; hence changing ice cover has a large control on surface solar absorption ($i.e.$, a positive feedback).

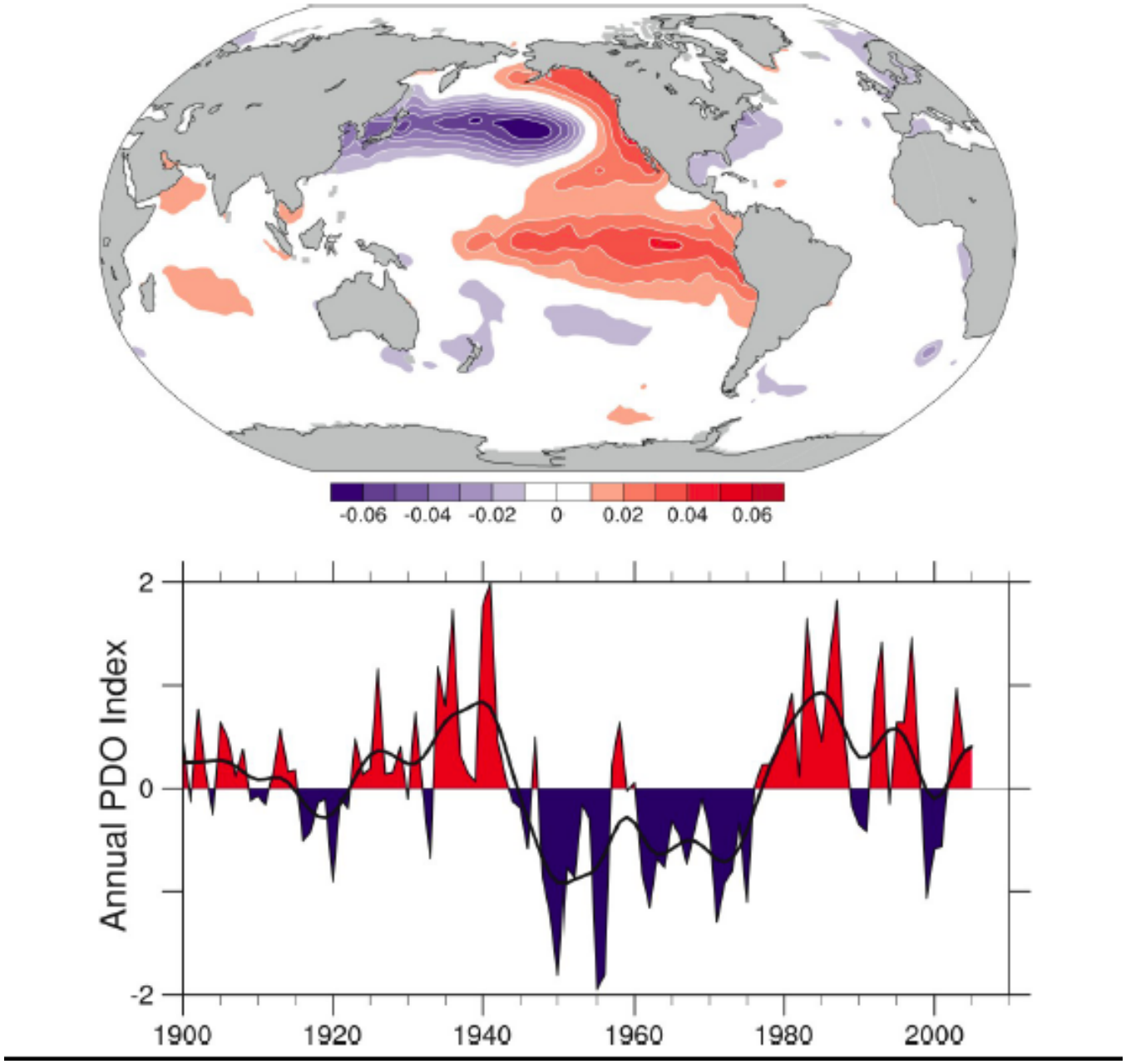

Pacific Decadal Oscillation (PDO): SST pattern and annual-anomaly time series. There is some spatial overlap with the ENSO SST pattern, but the time scale is much longer (decades).

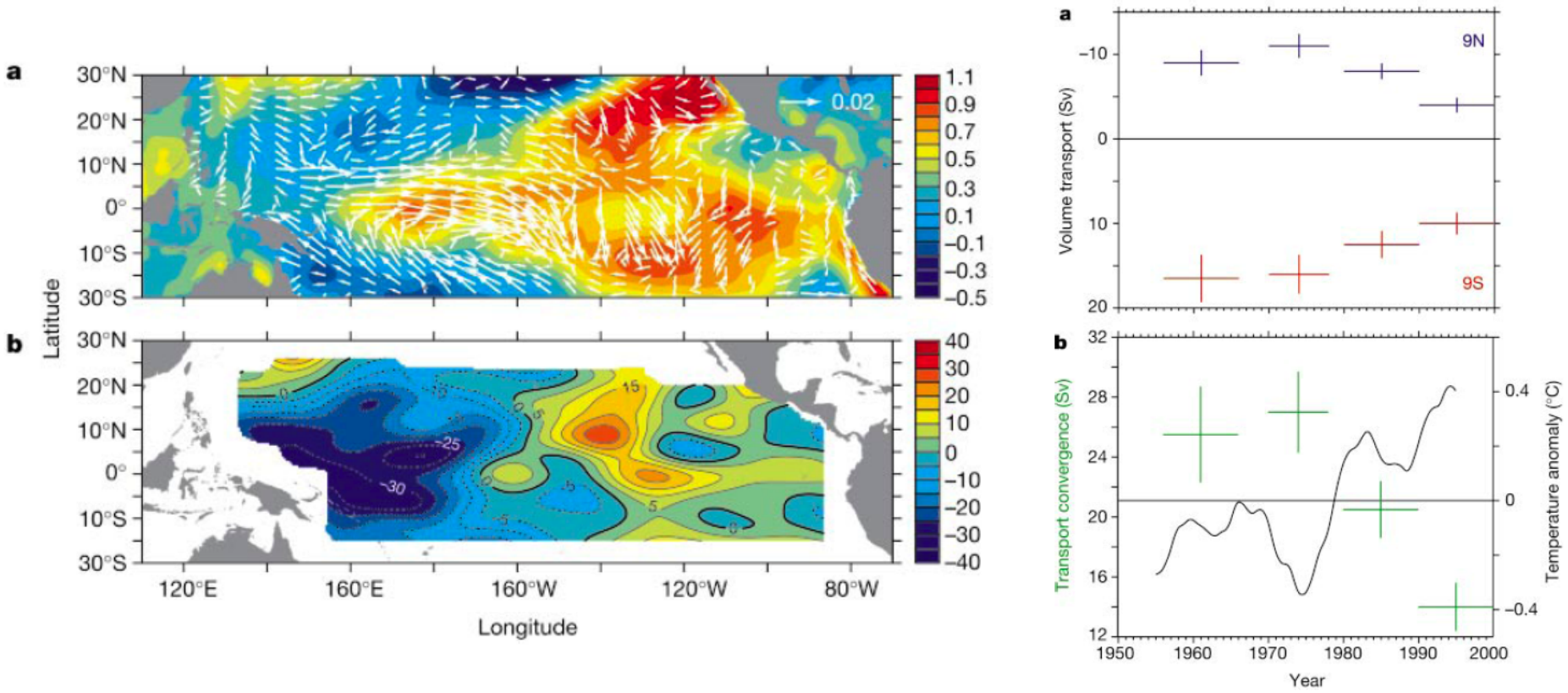

(Left) Decadal differences in wind stress [N m^{-2}], sea surface temperature, and isopycnal depth [m] ($\sigma_0 = 25.0$ kg m^{-3}) in the tropical Pacific between different phases of the PDO (1990-99 minus 1970-77). (Right) Time series of the weakening subtropical-cell MOC from 145E to the eastern boundary: (top) transports the Ekman layer ($\Rightarrow$ divergence) and (b) transport convergence in the thermocline. Also shown is a mean thermocline warming associated with weaker upwelling. Weaker trade winds diminish the circulation, hence the geostrophic zonal buoyancy gradients, hence shift the upper-ocean heat content toward the east. (McPhadden and Zhang, 2002)

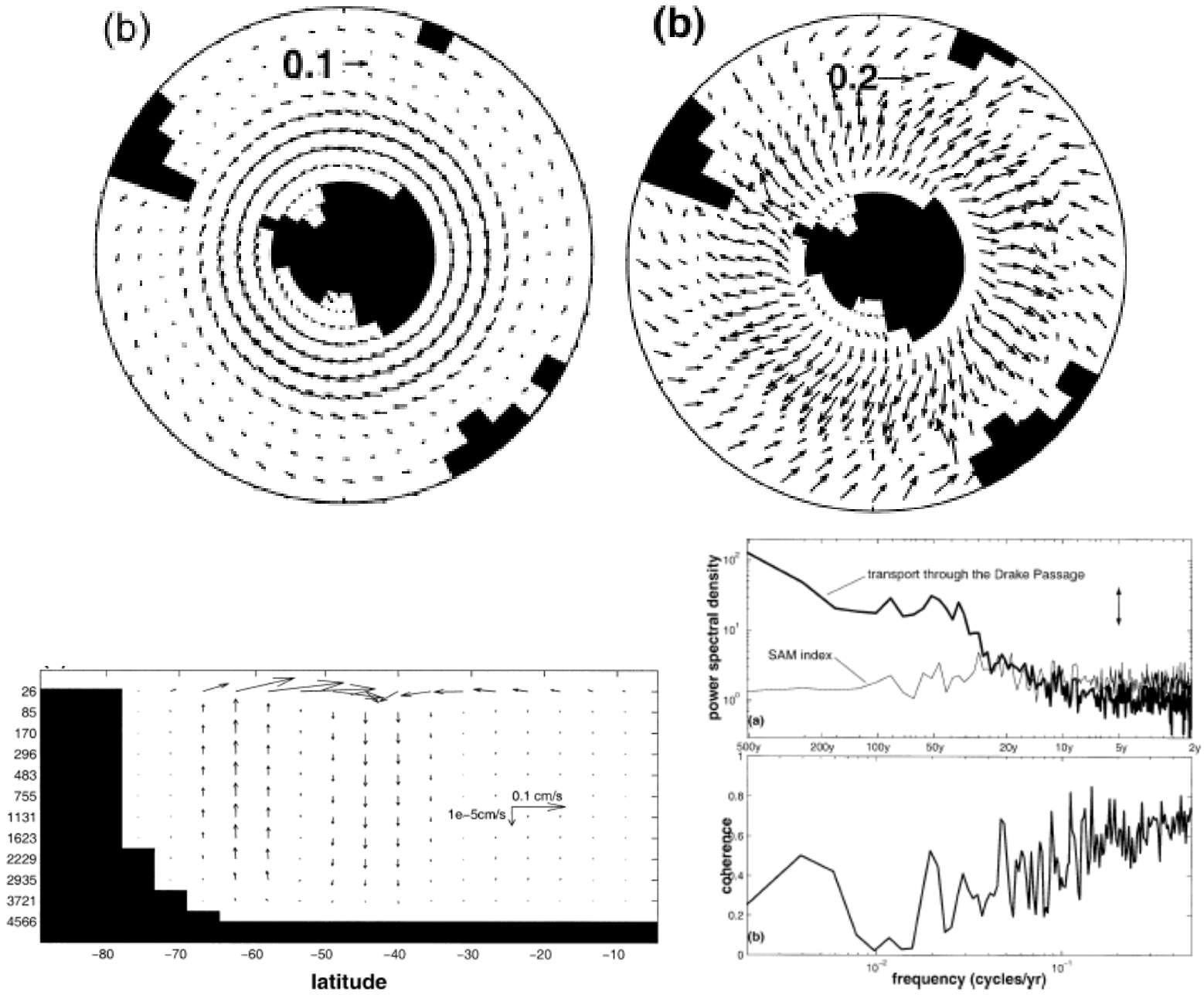

Southern Annular Mode (SAM) anomalies in an air-sea coupled model: wind, surface (Ekman) current, MOC, and frequency spectra in a coupled climate model. Notice that the ocean variables have relatively more low-frequency amplitude than the atmospheric ones. (Hall and Visbeck, 2002)

The Ocean as an Amplifier of Low-Frequency Climate Variability

Consider a simple model for atmospheric T_a and oceanic T_o temperature fluctuations in some unspecified spatially averaged sense:

$$\dot{T}_a = W - \alpha T_a + \lambda \frac{c_o}{c_a} [T_o - T_a] \quad (1)$$

$$\dot{T}_o = \lambda [T_a - T_o] , \quad (2)$$

where W is a white-noise forcing representing weather events; α^{-1} is an extra-tropical dynamical relaxation time towards the climatic mean state, $\mathcal{O}(10)$ days; c_a and c_o are atmospheric and oceanic heat capacities (with $c_o \gg c_a$ and $c_o \propto h$, the upper-ocean depth for active vertical mixing); and λ^{-1} is an air-sea thermal relaxation time whose magnitude is $\mathcal{O}(1)$ yr. The frequency spectra of T_o and T_a are much redder with coupling than that of T_a uncoupled. (Hasselmann, 1976)

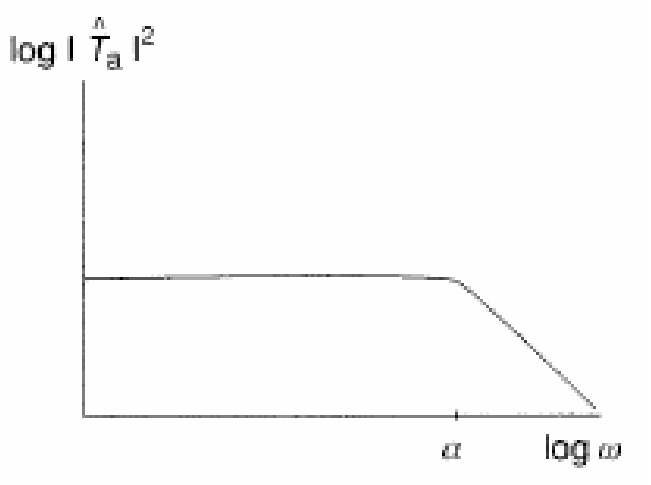

Uncoupled atmosphere with $T_o = 0$.

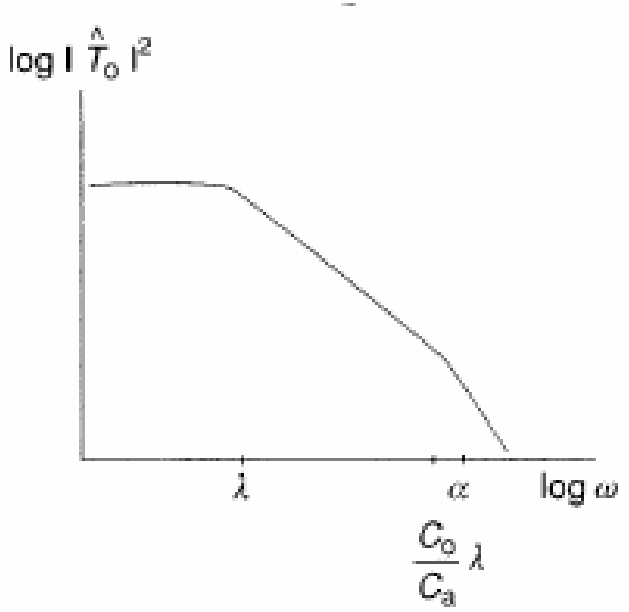

Coupled ocean. $|\hat{T}_a|^2(\omega)$ is also reddened.

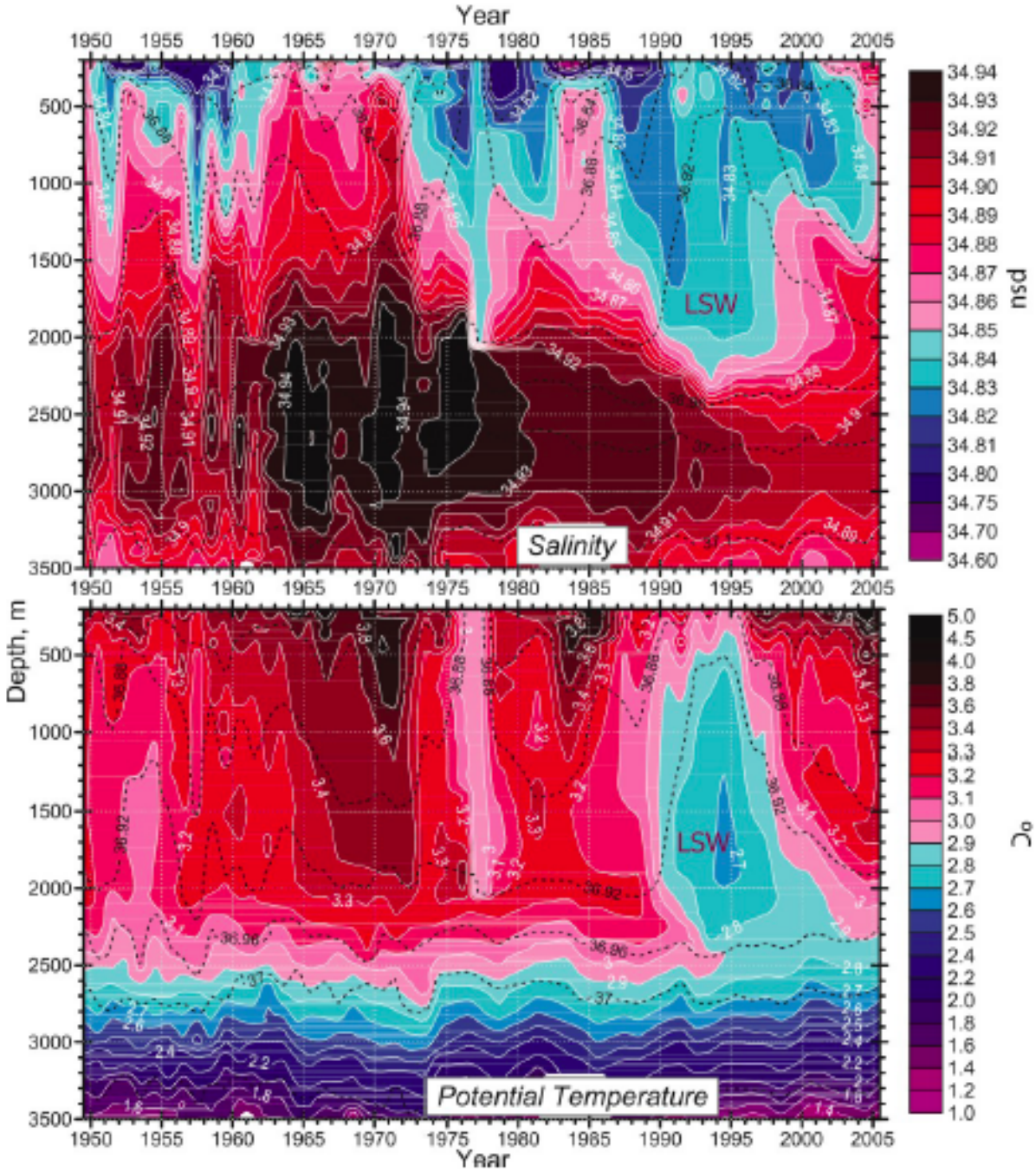

Time-series of S [PSU] and T [C] in the central Labrador Sea where deep wintertime convection often occurs. Notice the episodic "great salinity anomalies" at the surface and others at intermediate depth. These anomalies are advectively transported around the subpolar gyre, and are associated with reduced deep convection and NADW generation as well as variations in the North Atlantic Oscillation (NAO) in surface atmospheric fields. There is a positive correlation between S and T anomalies, indicating relatively smaller changes in density. (IPCC, 2007)

Empirical Orthogonal Functions

(a.k.a. Singular Value Decomposition or Principal Component Analysis)

purpose: given data in space-time, decompose it into a sequence of its most important spatial patterns, *i.e.*, in order of successively smaller contributions to the fluctuation data variance.

recipe:

- data are $u(\mathbf{x}_i, t)$ at locations $i = 1, ..., N$ and times t. (u denotes any variable.)
- subtract time mean at each point, $u' = u - \overline{u}$, and form fluctuation spatial covariance matrix, $C_{ij} = \overline{u'_i u'_j}$.
- determine eigenmodes and eigenvalues of C: $\sum_j C_{ij} e_j = \lambda_i e_i$, and order them as $\lambda_1 \geq \lambda_2 \geq \ldots \lambda_N \geq 0$.
- normalize spatially orthogonal eigenmodes, $\langle e_n e_m \rangle = \delta_{nm}$, where $\langle \cdot \rangle = N^{-1} \sum_i \cdot = Volume^{-1} \sum_i \cdot |d\mathbf{x}_i|$.
- expand data in EOFS: $u(\mathbf{x}_i, t) = \sum_{n=1}^{N} a_n(t) e_n(\mathbf{x}_i)$, where $a_n = \langle u e_n \rangle$. The modal amplitudes are temporally orthogonal and "optimally" approximate the total variance for any level of truncation $M < N$: $\overline{a_n a_m} = \lambda_n \delta_{mn}$ and $\langle \overline{u'^2} \rangle = \sum_{n=1}^{N} \lambda_n \approx \sum_{n=1}^{M} \lambda_n$.

usage: This is the most common approach to analyzing data with complex behavior when there is no good *a priori* idea what the patterns ought to be. Usually only the first few modes are considered important, and the remainder discarded (truncated at small M). Do not confuse space-time orthogonality with causal independence nor assume the EOFs are dynamically meaningful. (But people keep forgetting and/or hoping. (See HW #7, problem #3.)

EOFs of Real Data: Winter SLP anomalies

EOF 1: AO/NAM (23% expl).

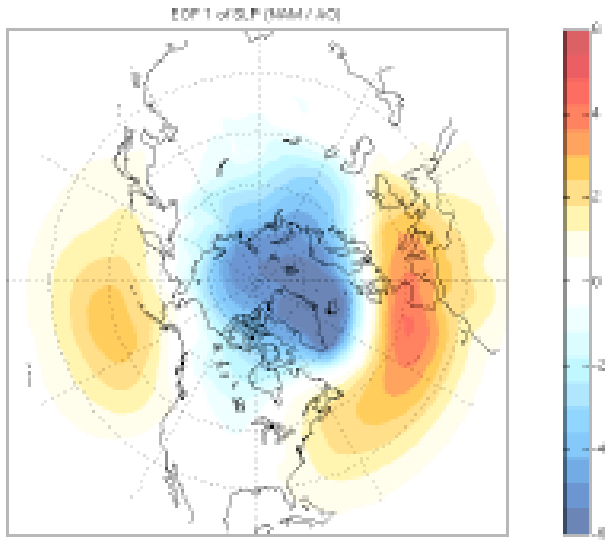

EOF 2: PNA (13% expl.)

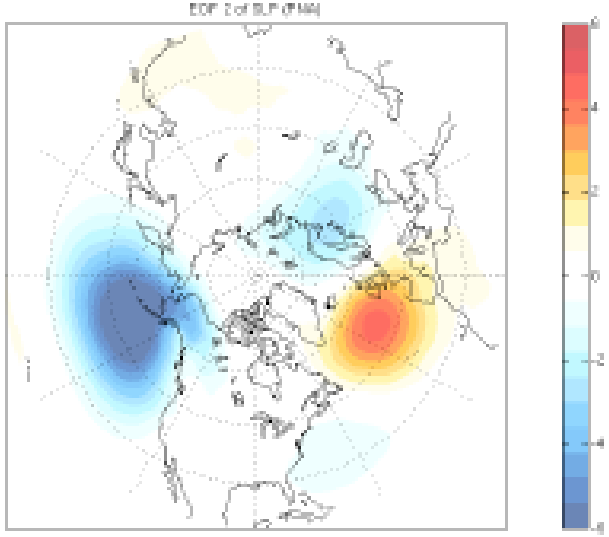

EOF 3: non-distinct(10% expl.)

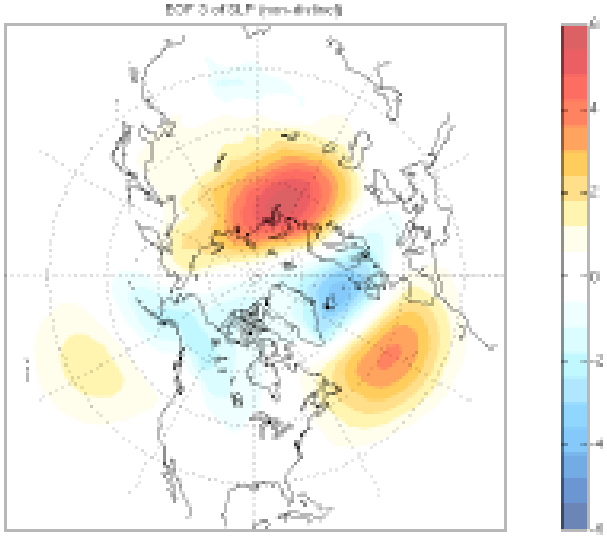

PC1 (AO/NAM)

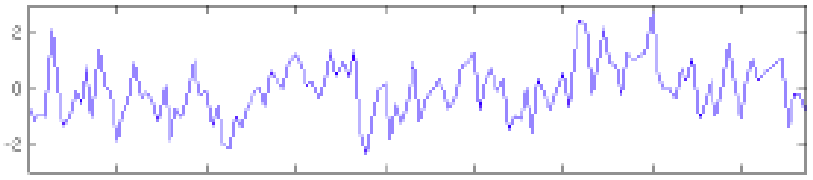

PC2 (PNA)

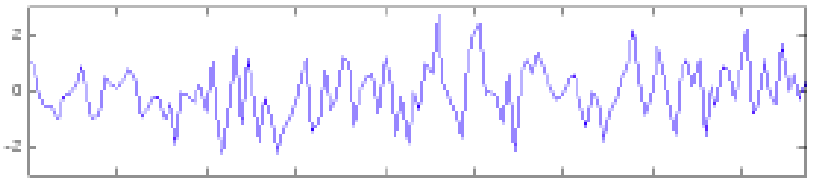

PC3 (?)

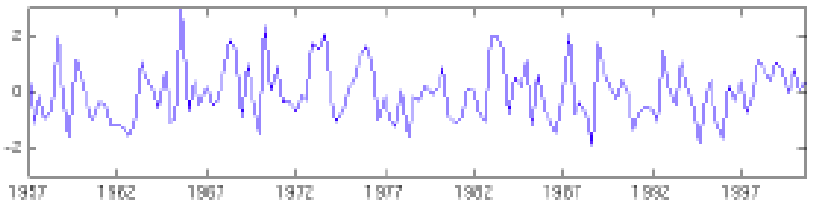

First 25 Eigenvalues for DJF SLP

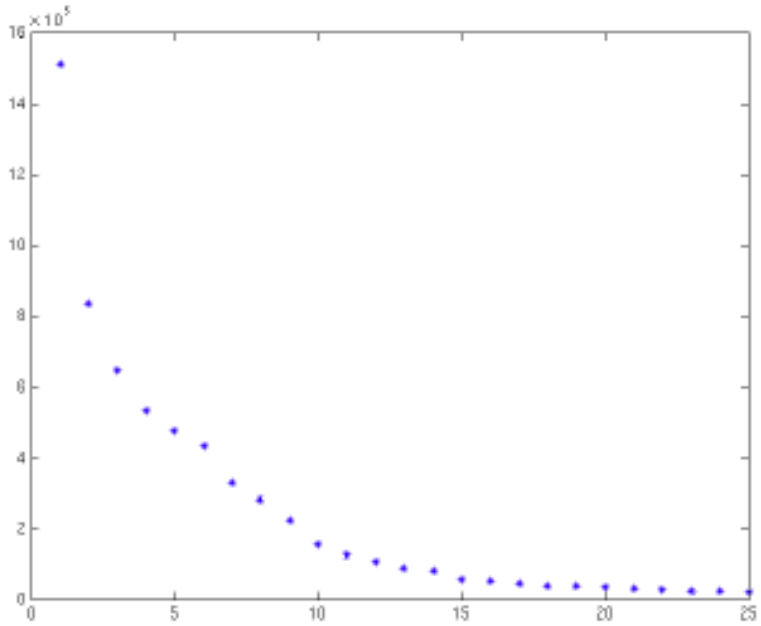

Paleoclimate indicators

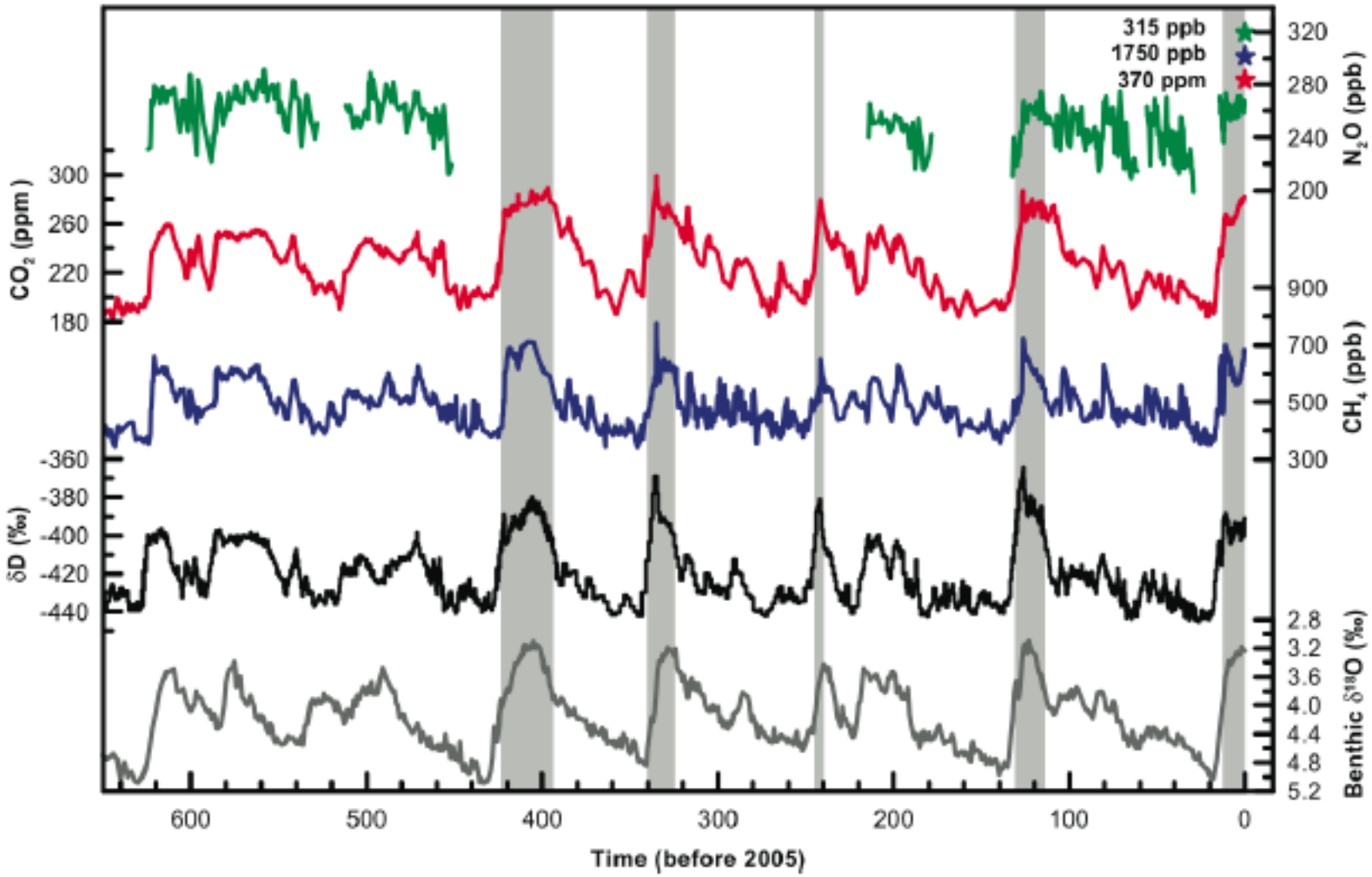

Over more than 600 ky large fluctuations occur in various chemical concentrations measured in land ice cores, indicating changes in atmospheric greenhouse-gas composition, ice volume, and temperature. Gray bands indicate warm periods like the present Holocene ($i.e.$, the most recent 10 ky).

A Paleothermometer: $\delta^{18}O$

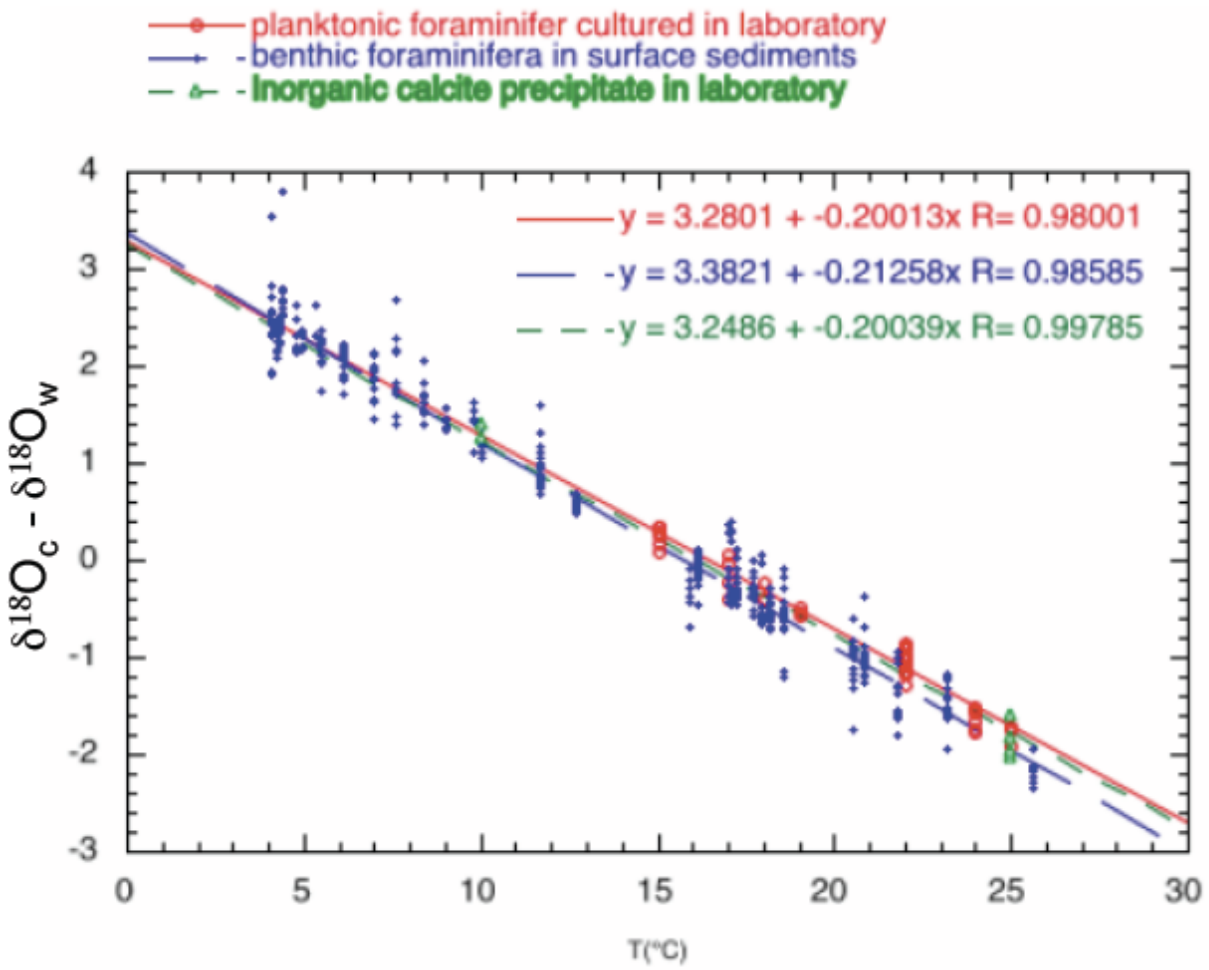

The isotope ratio of oxygen atoms ($^{18}O/^{16}O$) in CaCO3 relative to water, versus temperature. The $\delta^{18}O$ (normalized $^{18}O/^{16}O$ ratio) is greater than the CO_3^{2-} from which it's formed (which depends on that of H_2O), bu the difference decreases by ~0.1% for every 5 degree increase in temperature. Changes in the ratio can be used (with caution) as a thermometer.

A Paleothermometer: Faunal Assemblages

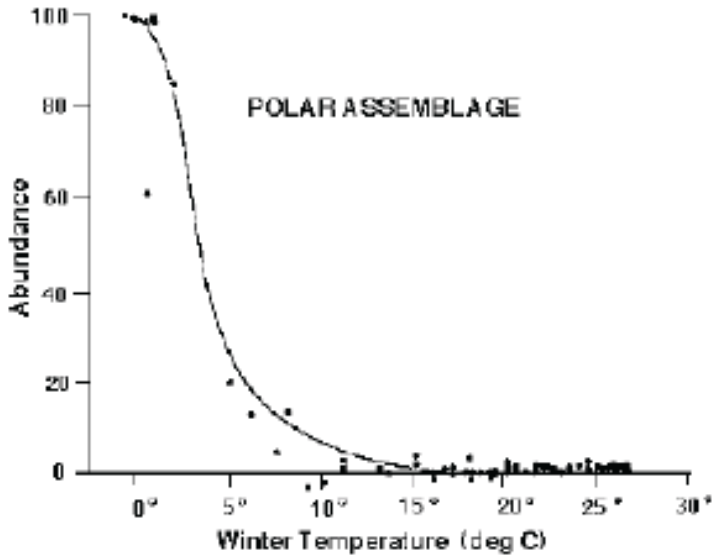

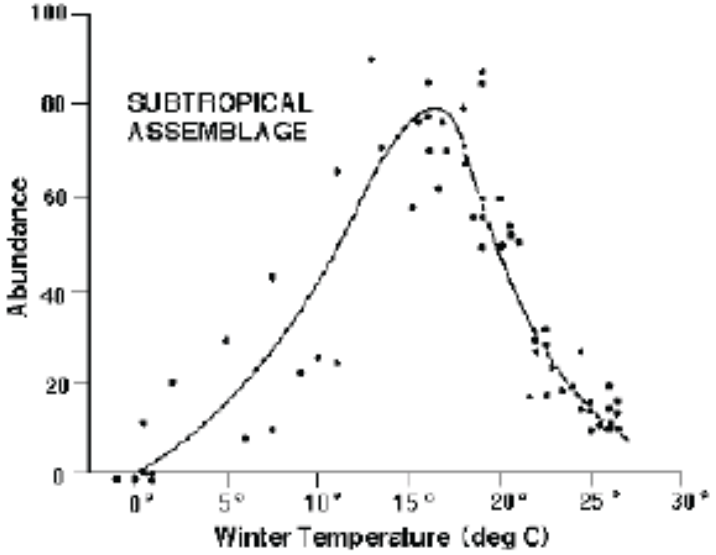

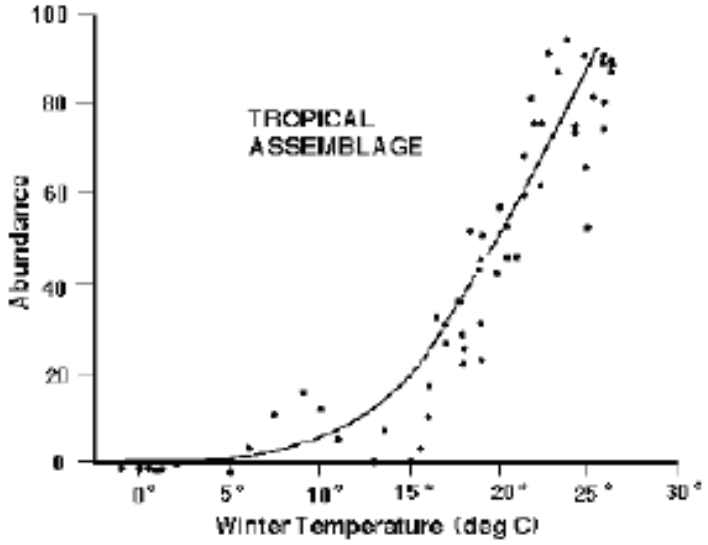

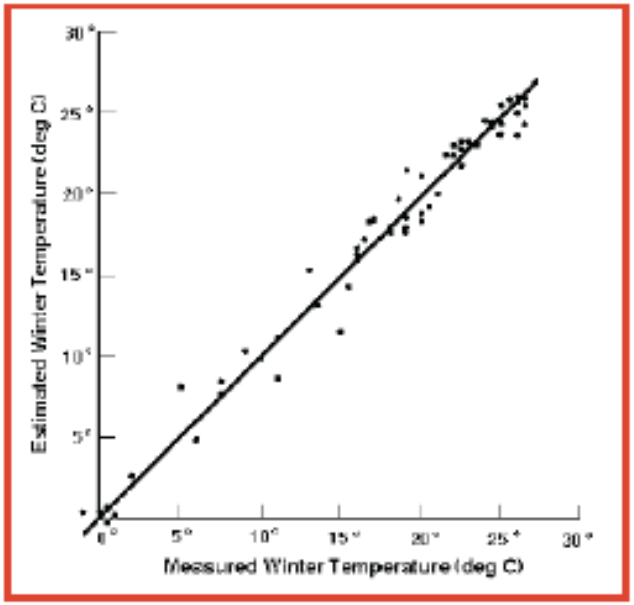

Surface-dwelling plankton communities can be grouped into "assemblages" according to thermal niche (analogous to other identifications of functional groups of common ecological behavior). Changes in the distribution of these assemblages in paleo-sediments can be used to estimate SST.

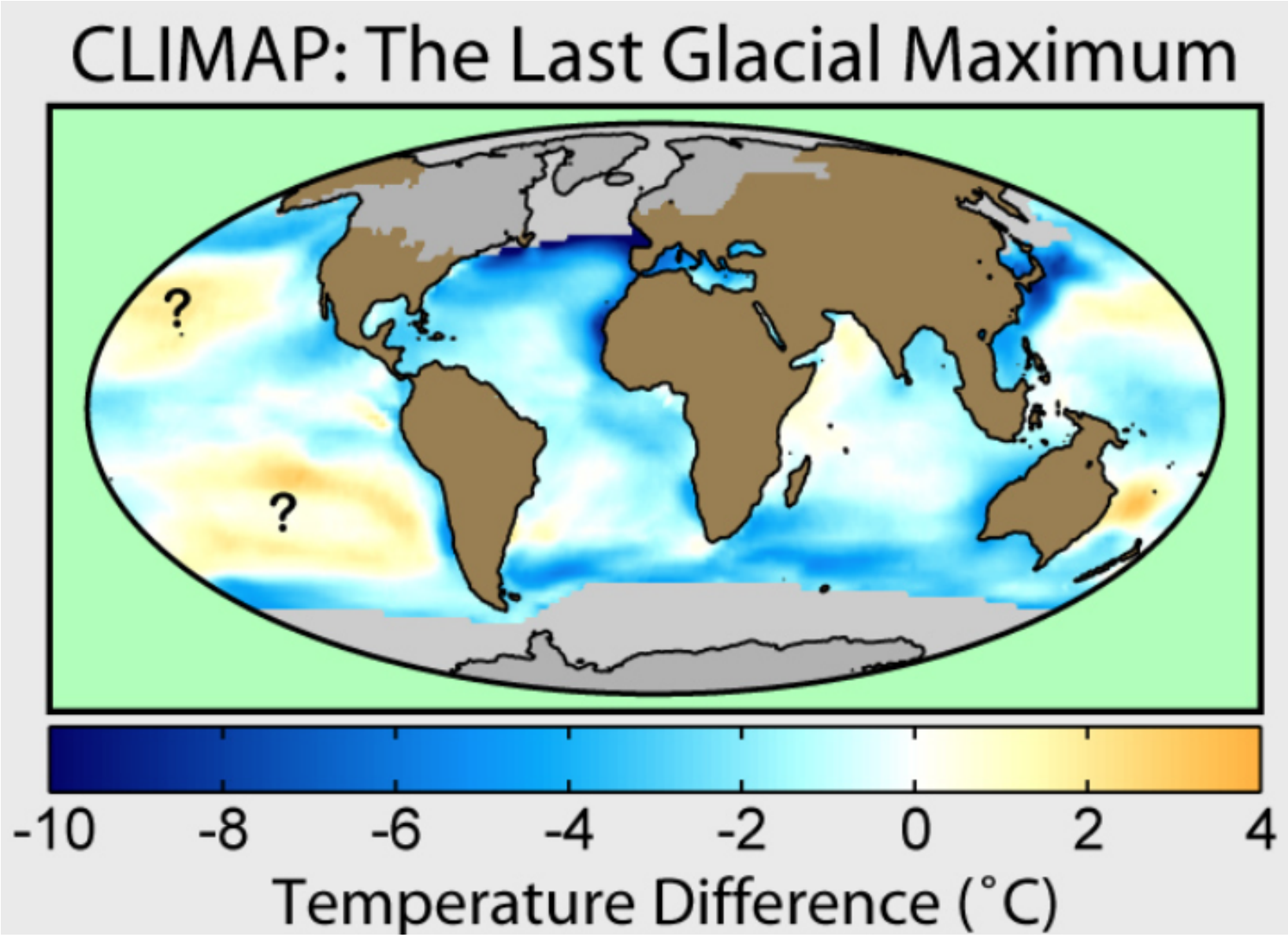

An estimate of the change in SST between now and the last glacial maximum around 25 ky BP based on faunal assemblages. This was an early result from the CLIMAP program in the 1970s, and subsequent revisions have been made. Clearly the polar regions were colder, equatorward of the expanded sea-ice zones. The tropical regions were somewhat ambiguously different, but mostly a bit cooler.

Water Column Proxy Relations

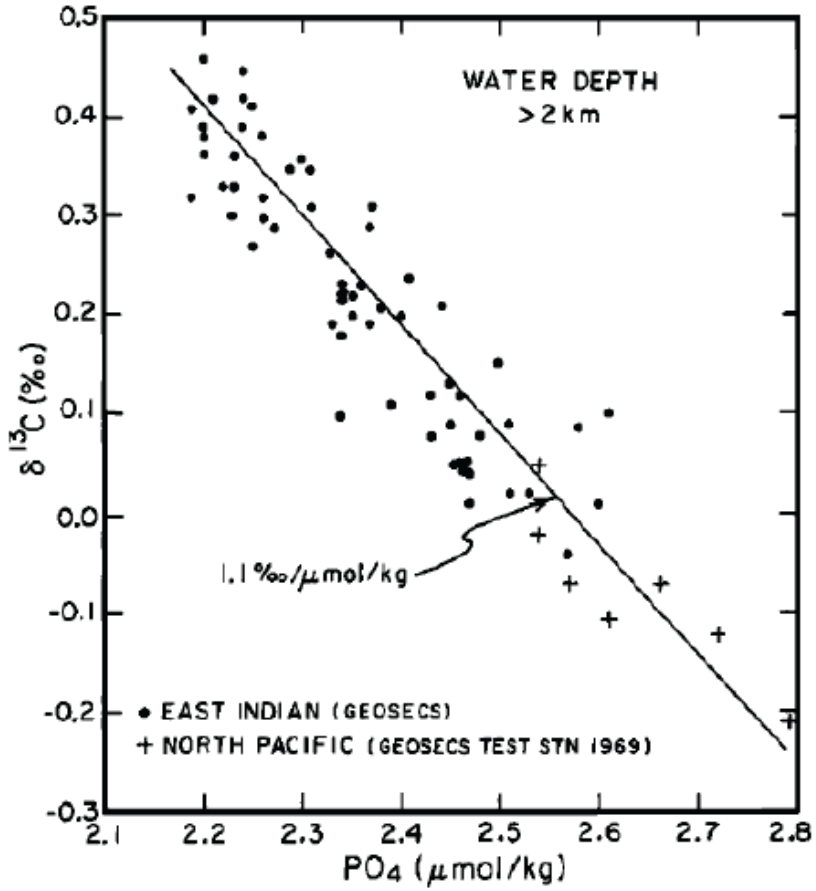

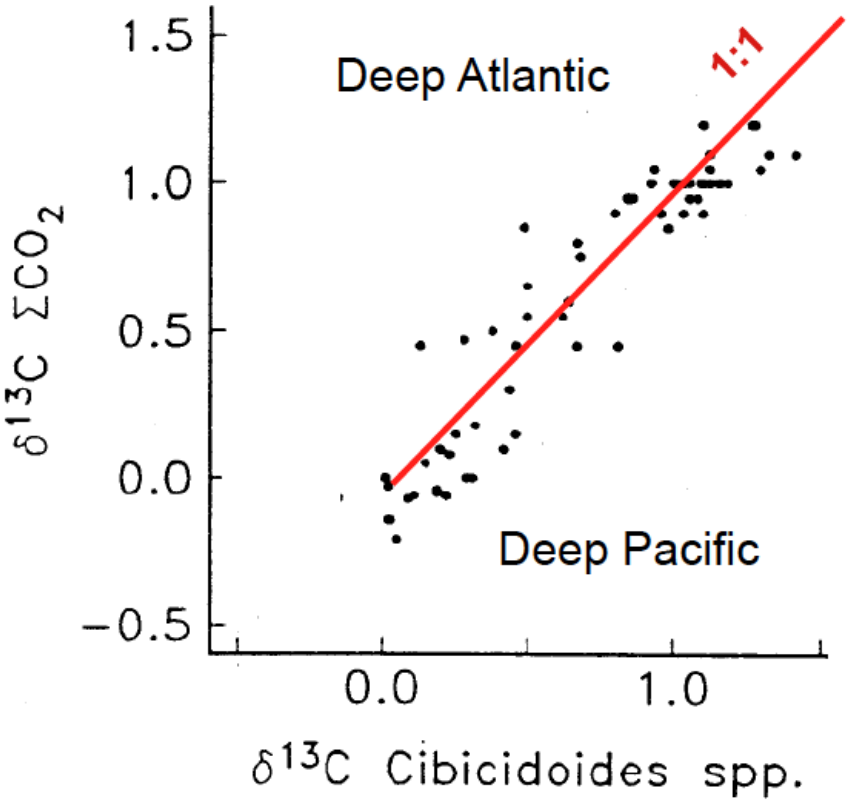

Water mass tracers exploit the empirical relations between $\delta^{13}C$ and a primary nutrient PO_4 (left) — a mirror relation because photosynthesis that depletes PO_4 consumes ^{12}C faster than ^{13}C and remineralization does the reverse — and a benthic foraminifera (right). This allows paleo-sediment faunal measurements of $\delta^{13}C$ to be used to diagnose PO_4 concentration.

Glacial Deep Atlantic

Western Atlantic GEOSECS $\delta^{13}C$ (PDB)

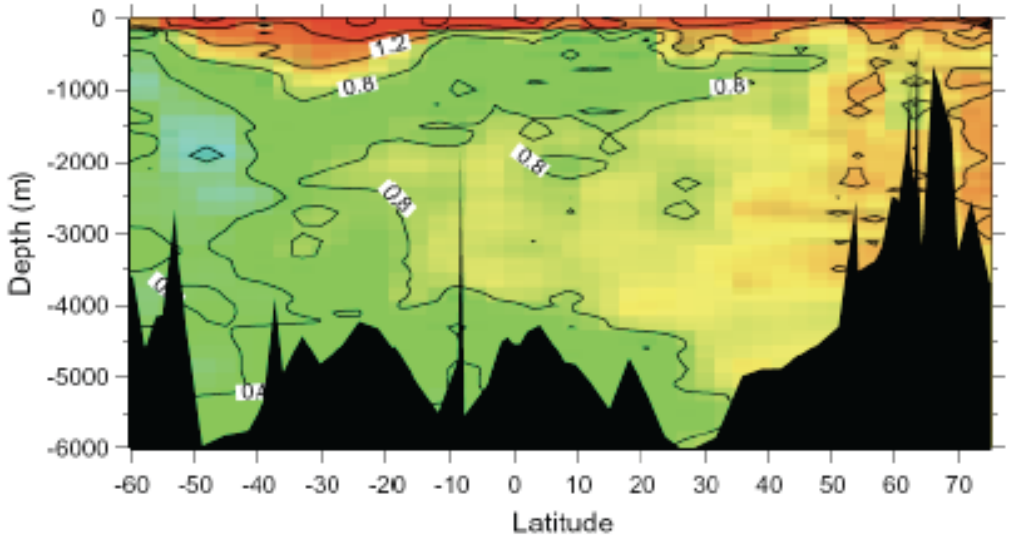

Western Atlantic Glacial $\delta^{13}C$ (PDB)

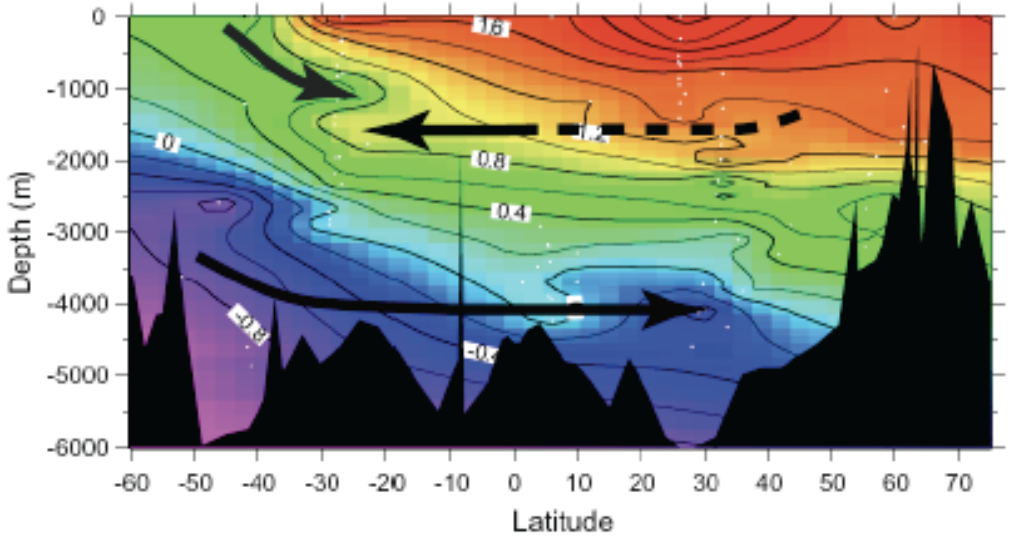

Modern and glacial $\delta^{13}C$ distributions from the Western Atlantic. Glacial values are reconstructed from multiple sediment cores (small white dots). Interpretation: low-nutrient NADW was much shallower and high nutrient AABW was more extensive than now.

Curry and Oppo [2005]

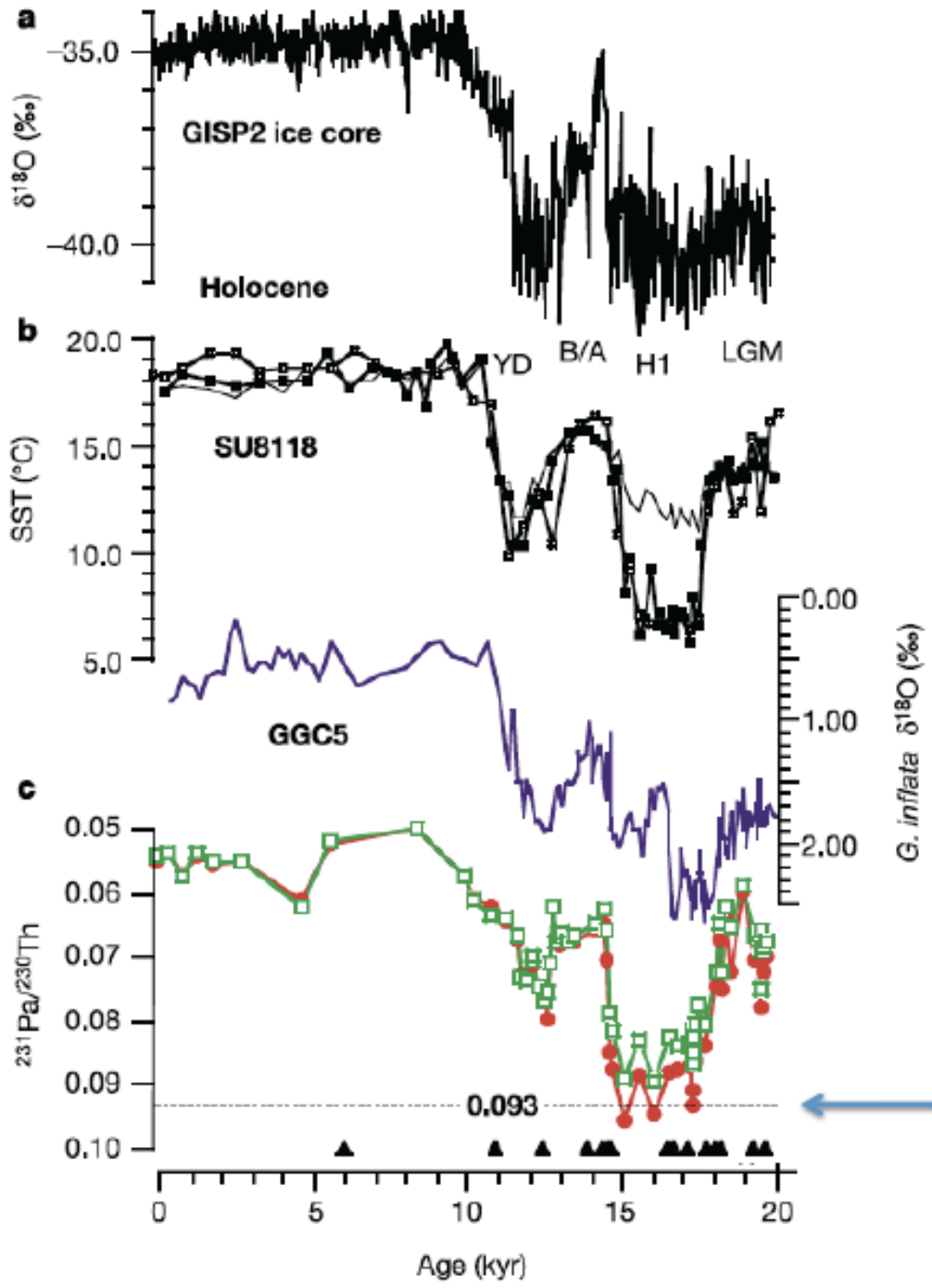

Sediment proxies from the North Atlantic at start of the interglacial period, supporting the idea of melt-water pulses slowing the NADW formation rate and cooling the North Atlantic. [McManus et al., 2004]

Proxy for circulation rate.
If sediment ratio is ~ production ratio (0.093), this indicates water stagnation.

Glacial deep Pacific

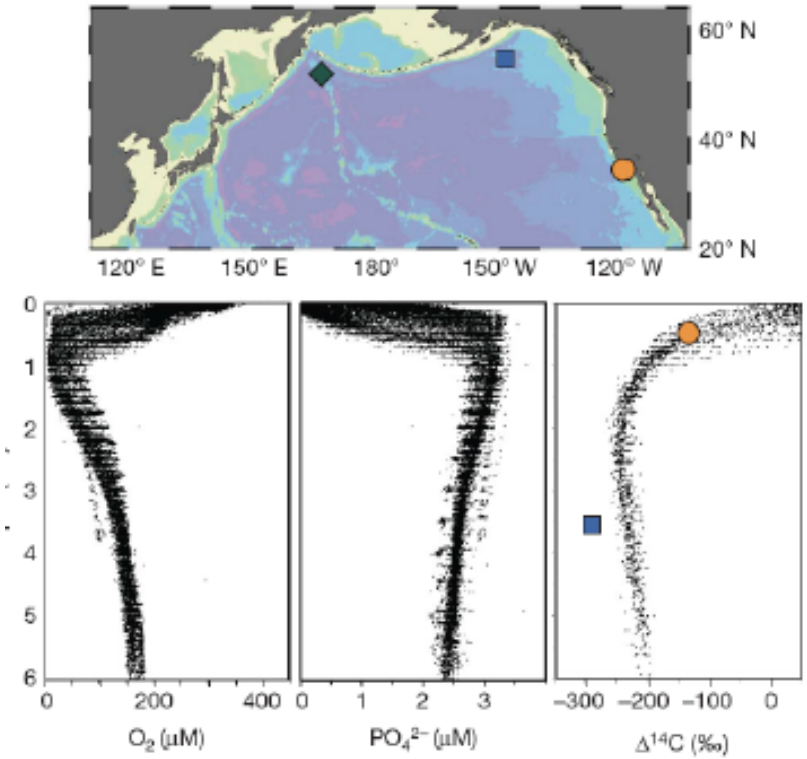

Galbraith et al. [2008]

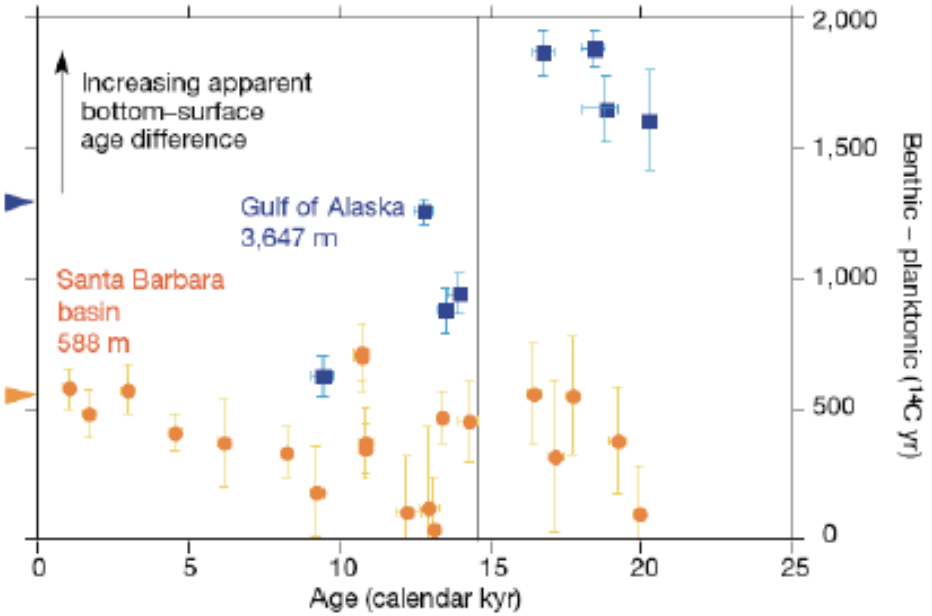

Figure 2 | Apparent age differences between paired benthic and planktonic foraminifera at intermediate and deep sites in the North Pacific over the past 25 kyr. Published data from the upper ocean are shown by dark yellow circles, using the published age model[14]. New data from ODP Site 887 are shown as dark blue squares. Differences are calculated from the raw, measured ^{14}C ages. Estimated pre-industrial values for both sites are indicated by the triangles at the left-hand side. The calendar ages used here are the calibrated planktonic ages. Errors are $\pm 1\sigma$ and include errors in the ^{14}C measurement, calendar age calculation and reservoir age. The vertical grey line is drawn at 14.6 kyr ago, as in Fig. 3.

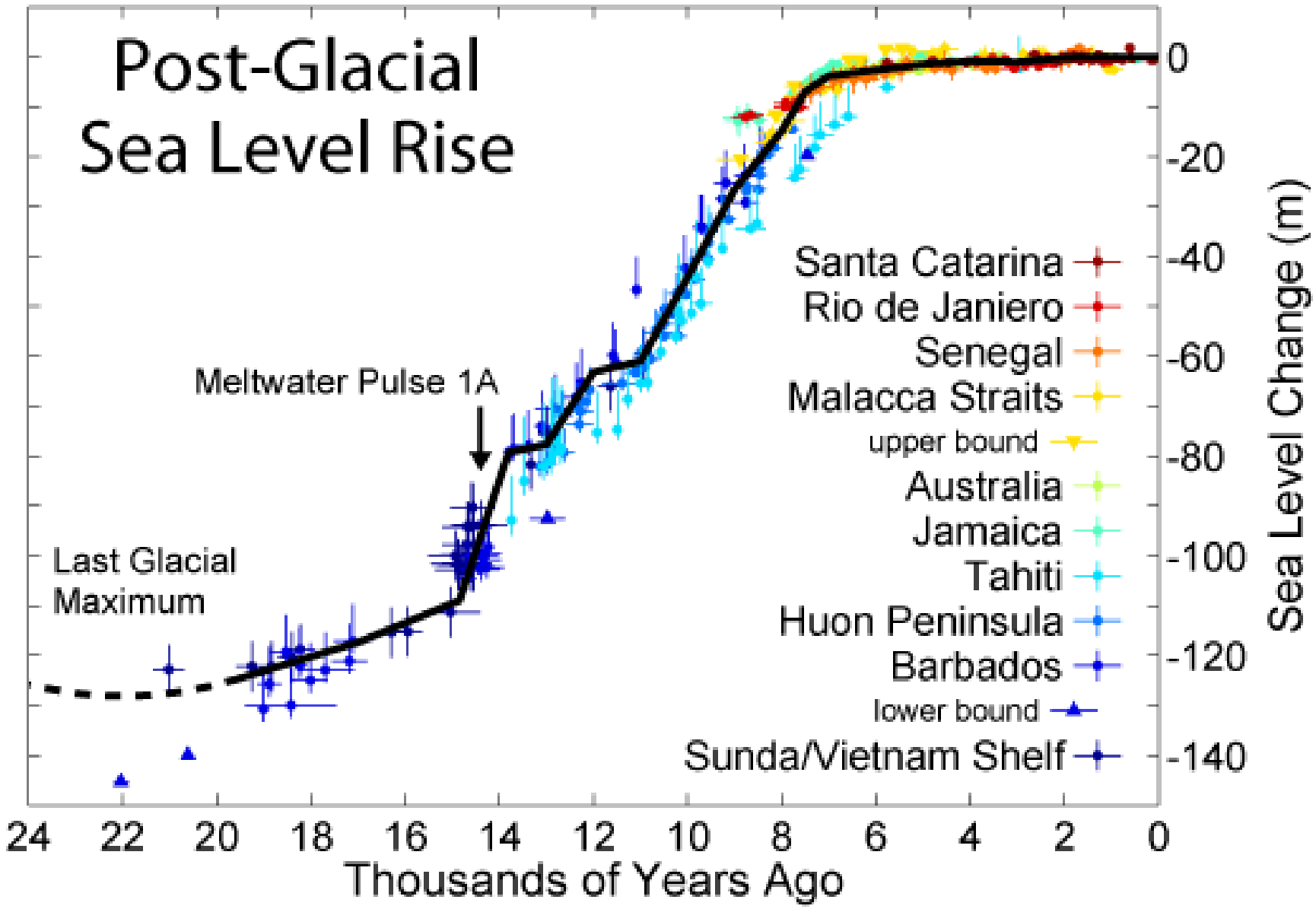

Estimates of global sea level over the transition from the Last Glacial Maximum through the present Holocene period. This increase is due mostly to ice-age land-ice melt. ((`http://en.wikipedia.org/wiki/Current_sea_level_rise`)

Anthropogenic Climate Change

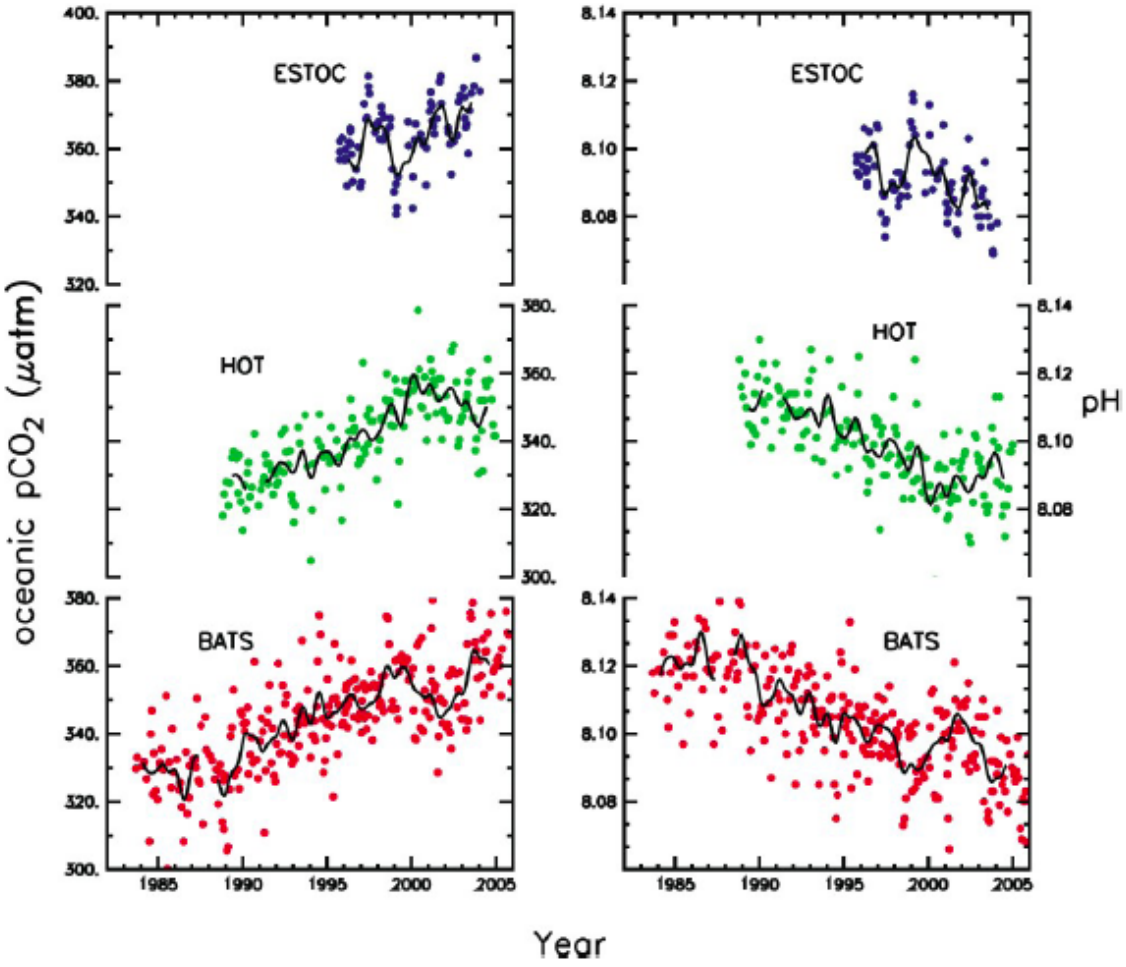

Time-series of surface oceanic pCO_2 [μatm] and pH at three locations: ESTOC (29 N, 15 W), Hawaii Ocean Time-series (HOT; 23 N, 158 W), and Bermuda Atlantic Time-series Study (BATS; 31 N, 64 W). The mean seasonal cycle was removed from all data. (IPCC, 2007) This figure is repeated.

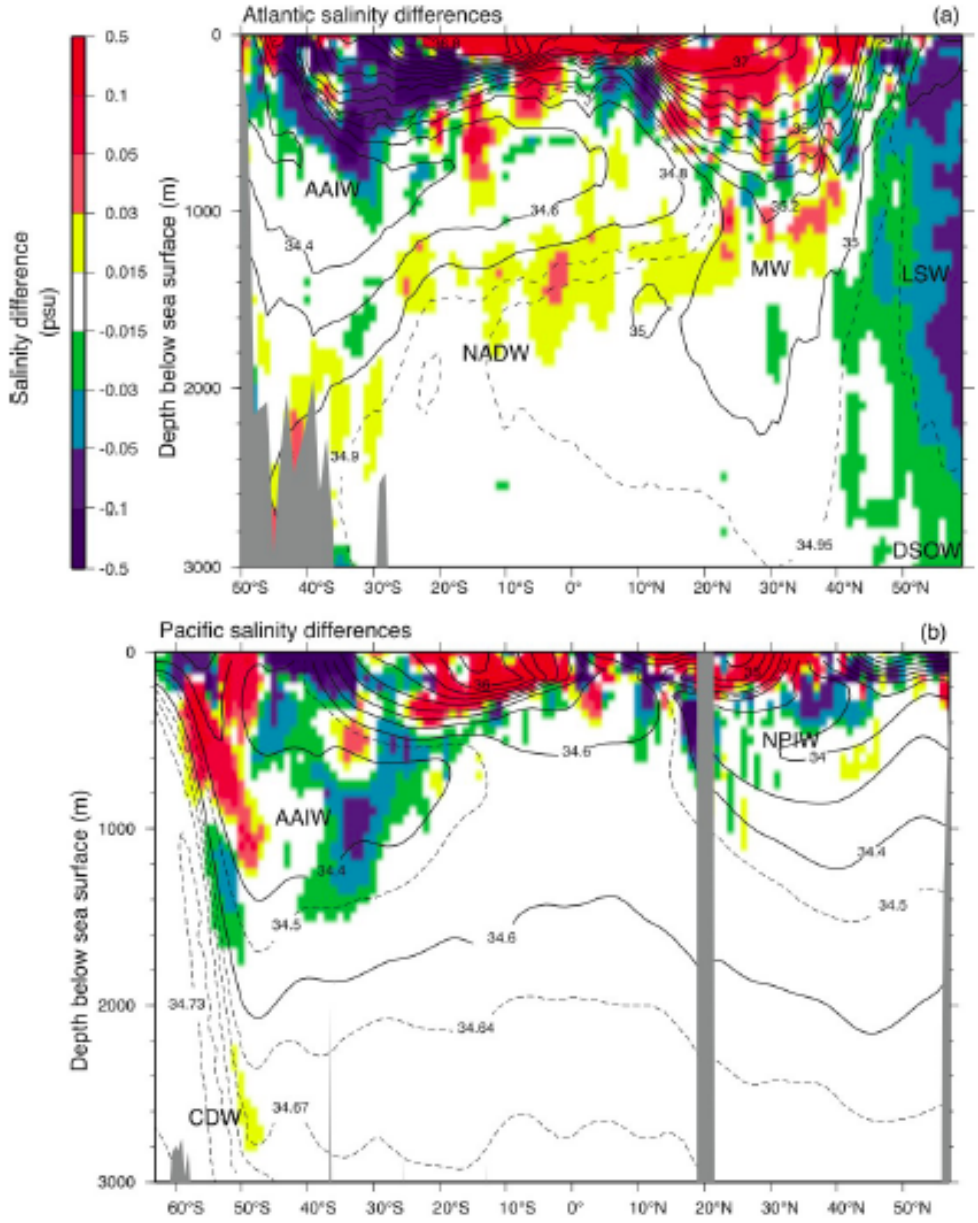

Salinity changes on Atlantic and Pacific sections between 1955-1969 and 1985-1999. Subtropical increases and subpolar decreases are consistent with intensification of the hydrological cycle. Freshening at intermediate water formation regions and subsequent isopycnal spreading increases stratification, adding to the effects of warming. (IPCC, 2007)

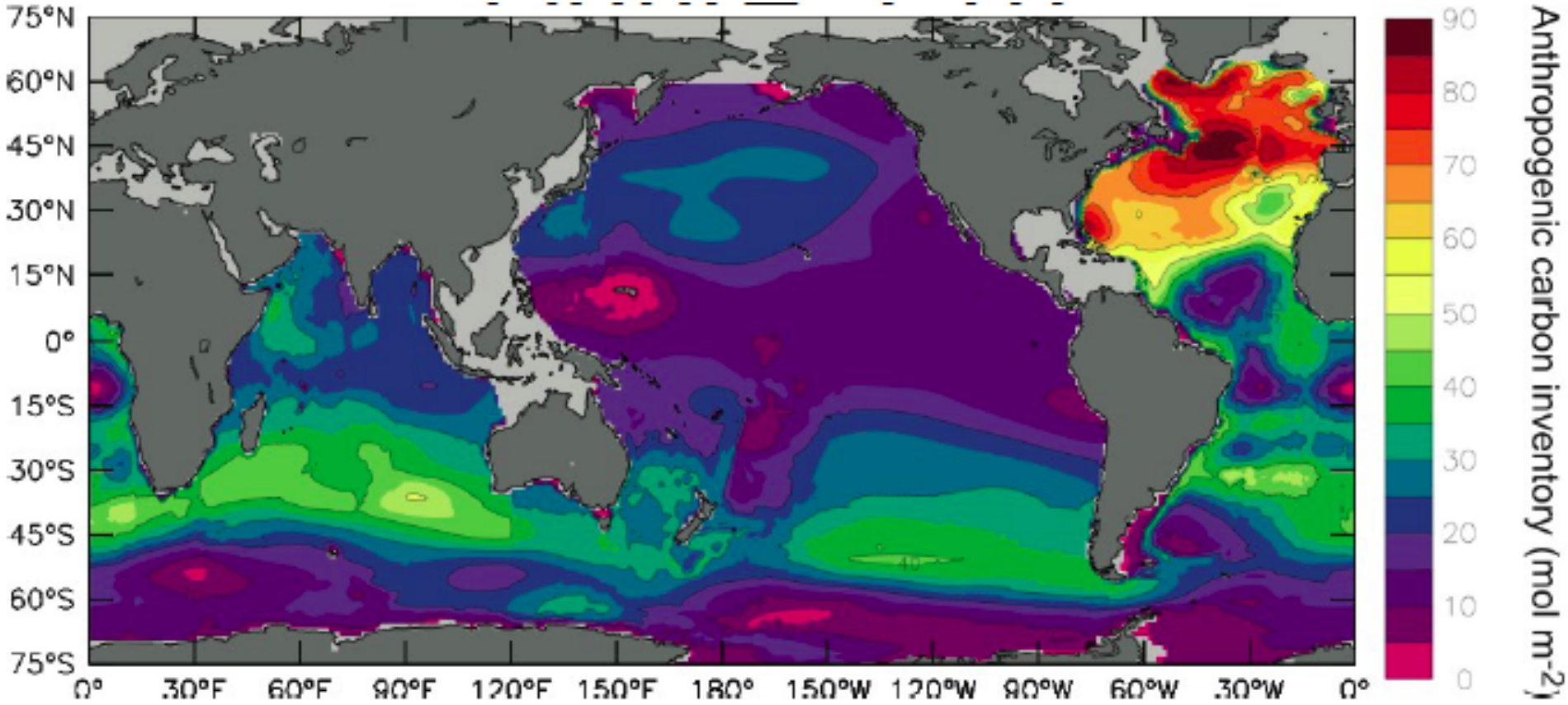

Column inventory of anthropogenic C [mol m^{-2}] as of 1994. Notice the high invasion in the sub-Antarctic and North Atlantic because of downwelling, ventilation, and subduction. (In general CO_2 uptake is largest where there is upwelling due to undersaturation, but this is not the same as inventory; see slide #30 two ahead.) (Sabine *et al.*, 2004)

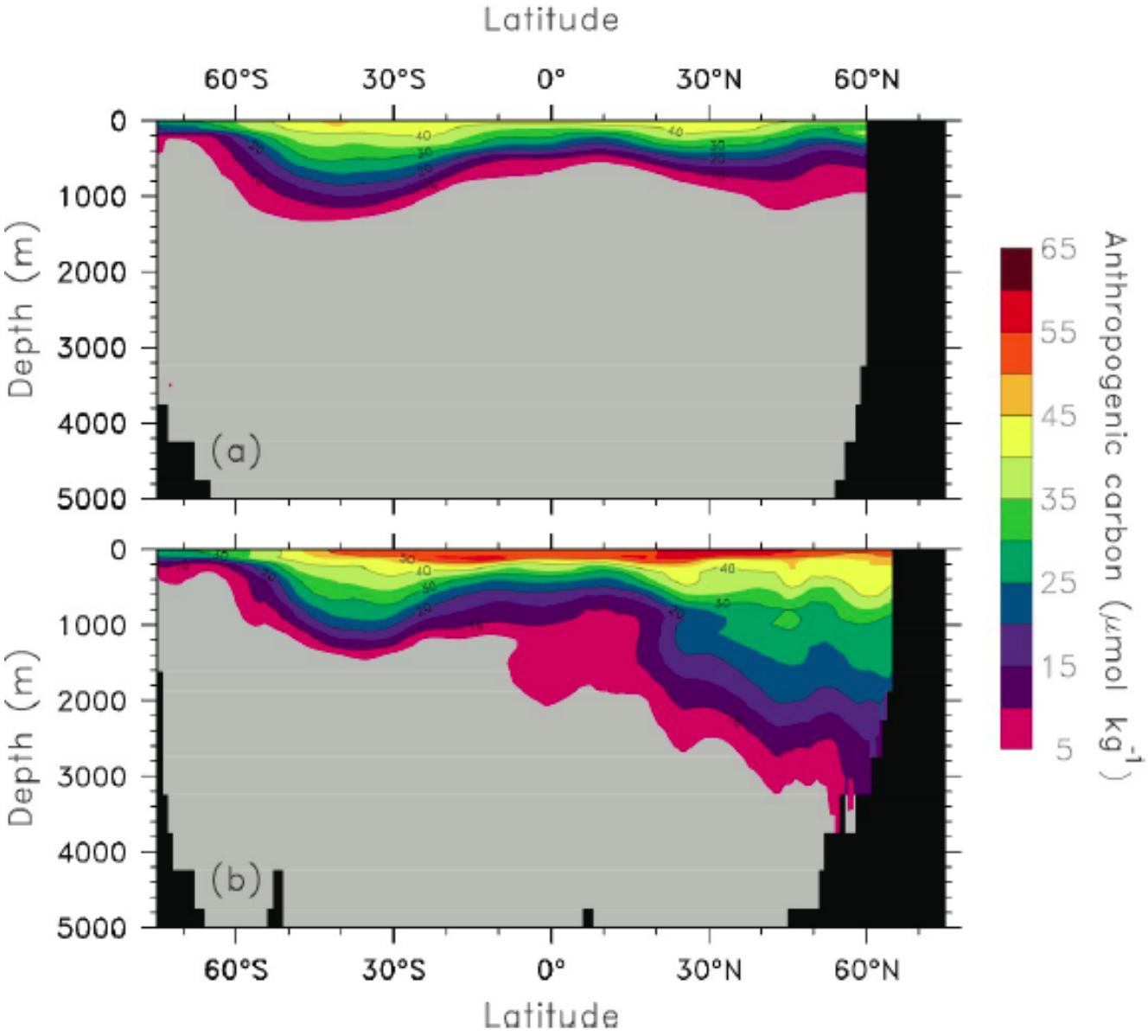

Mean concentration of anthropogenic C [μmol kg^{-1}] as of 1994 in the Indo-Pacific and Atlantic Oceans. The invasion is downward from the surface, with greater penetration in the subtropical gyre "bowls" (mode water) and in the North Atlantic Deep Water formation zone. (Sabine $et\ al.$, 2004)

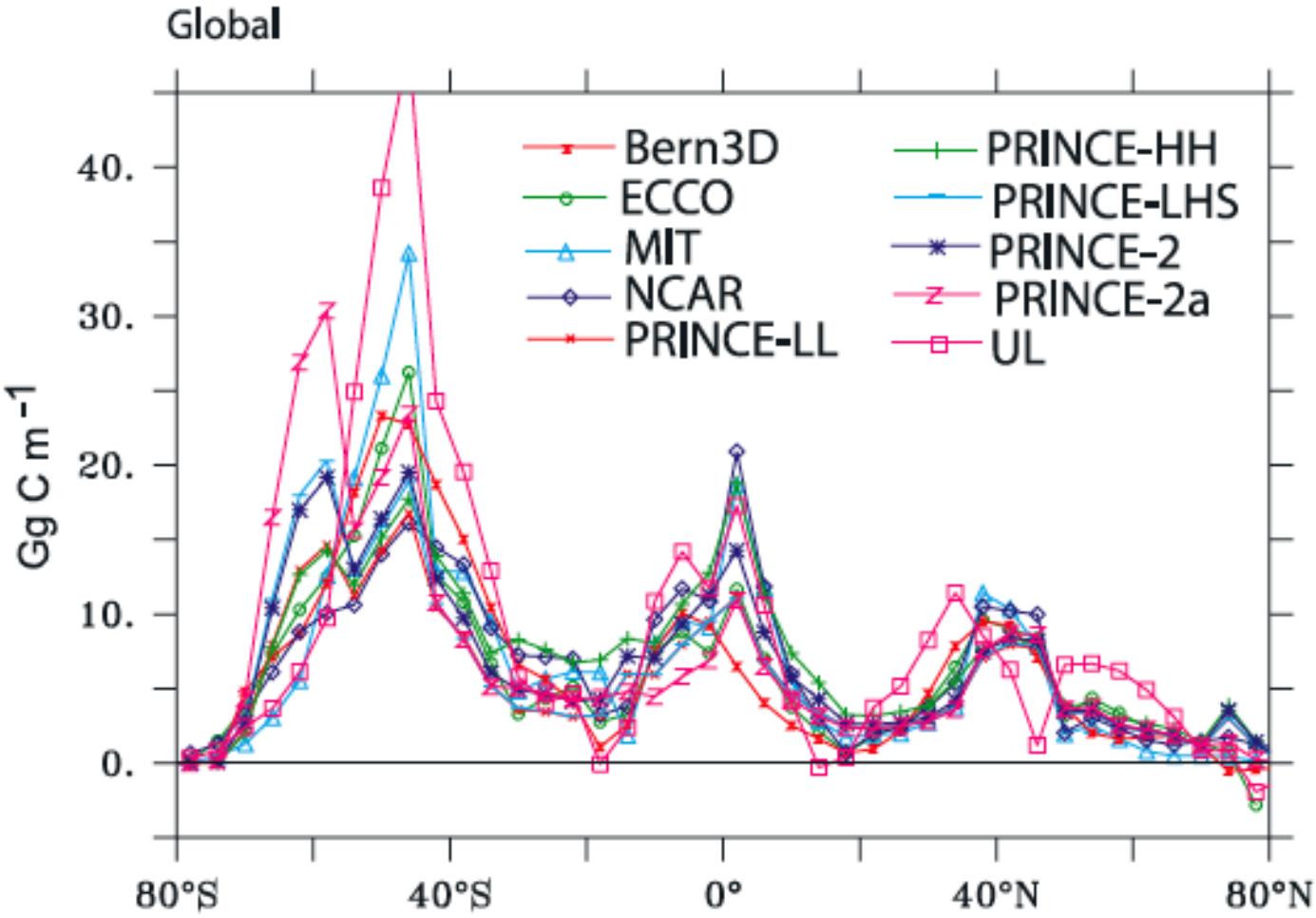

General circulation model estimates of the zonal mean oceanic uptake of anthropogenic CO_2 rescaled in time to the year 1995 (Mikaloff Fletcher *et al.*, 2006). The rate-limiting process in the uptake is the exchange between the mixed layer and the ocean interior, so the model differences are due primarily to the underlying ocean circulations.

It is typical of GCM simulations of global change that there is considerable spread among different models' answers because of chaotic behaviors, non-fundamental parameterization design choices among models, and rough parameter dependencies (McWilliams, 2007).

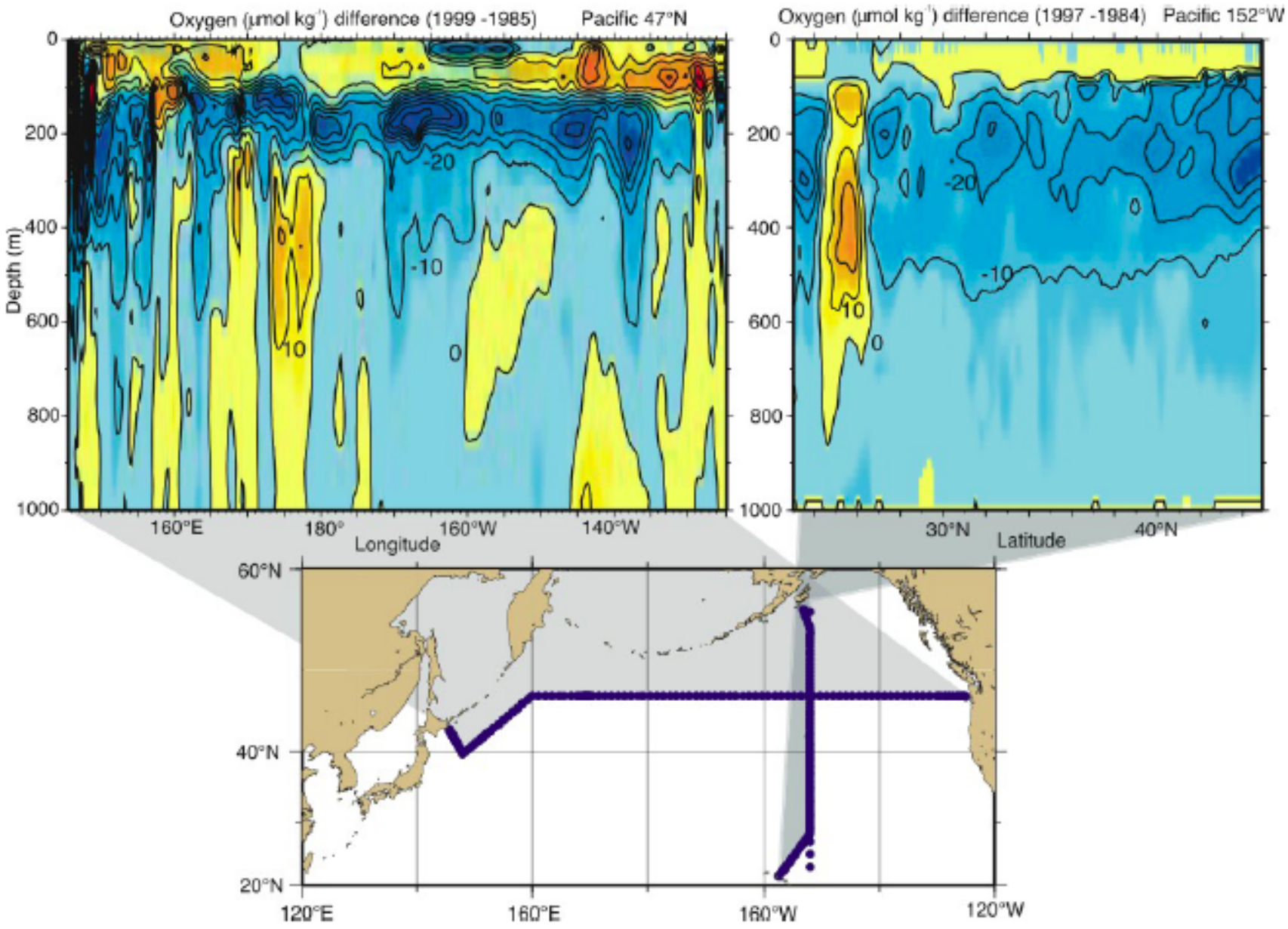

Changes in O_2 concentration [μmol kg^{-1}] between the 1980s and 1990s along two sections in the North Pacific. Decline in thermocline O_2 between decadal surveys is consistent with the slowing of ventilation rates, as expected from increased stratification. Ventilation is responsible for supplying O_2 to the ocean interior to compensate for respiration. (Deutsch *et al.*, 2005)

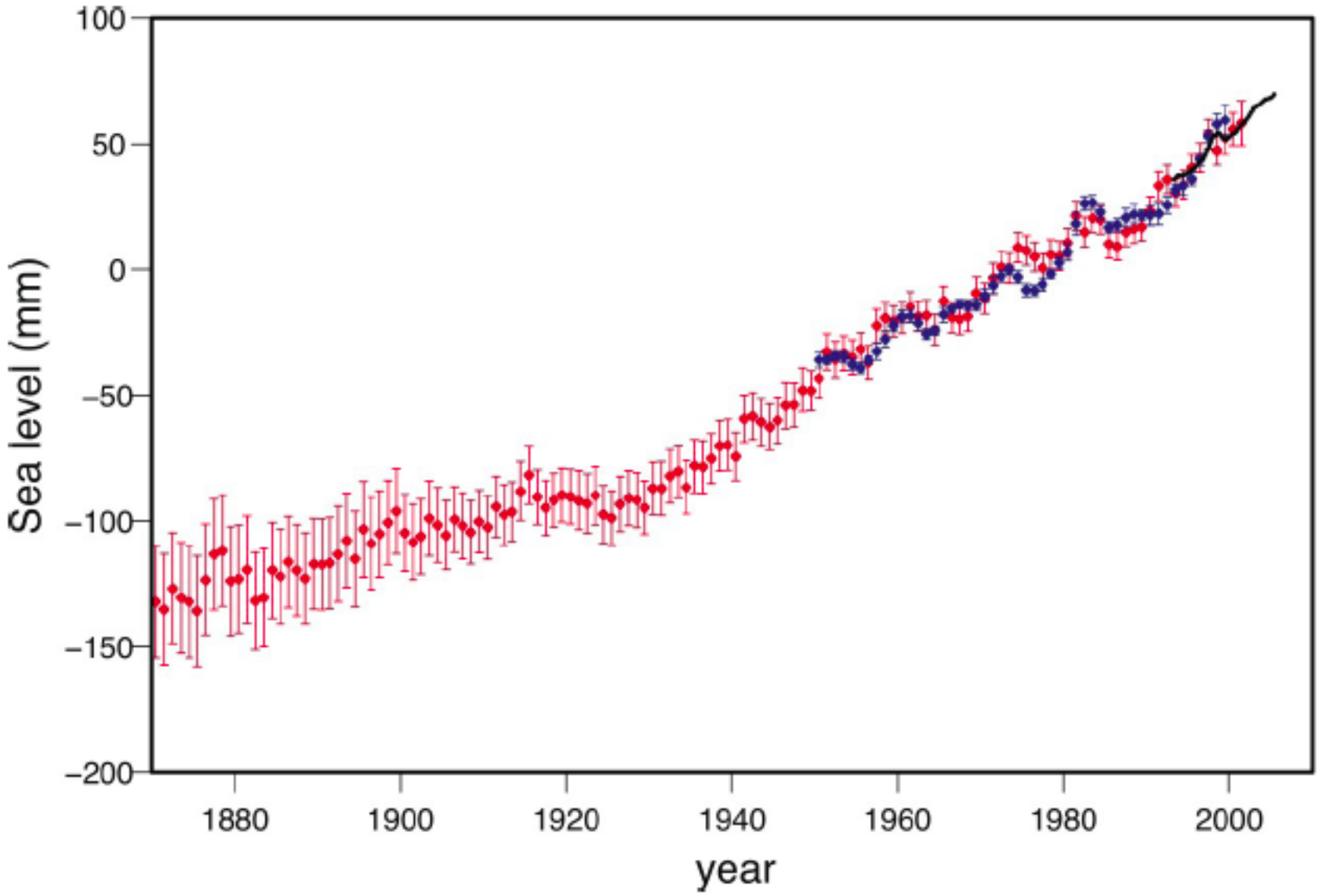

Annual averages of global-mean sea level changes due primarily to steric height (sea water expansion due to warming) and secondarily to land ice volume decrease through melting. Red is from tide gauges; blue is from hydrography; and black is from satellite altimetry (IPCC, 2007). The rate of increase is accelerating.

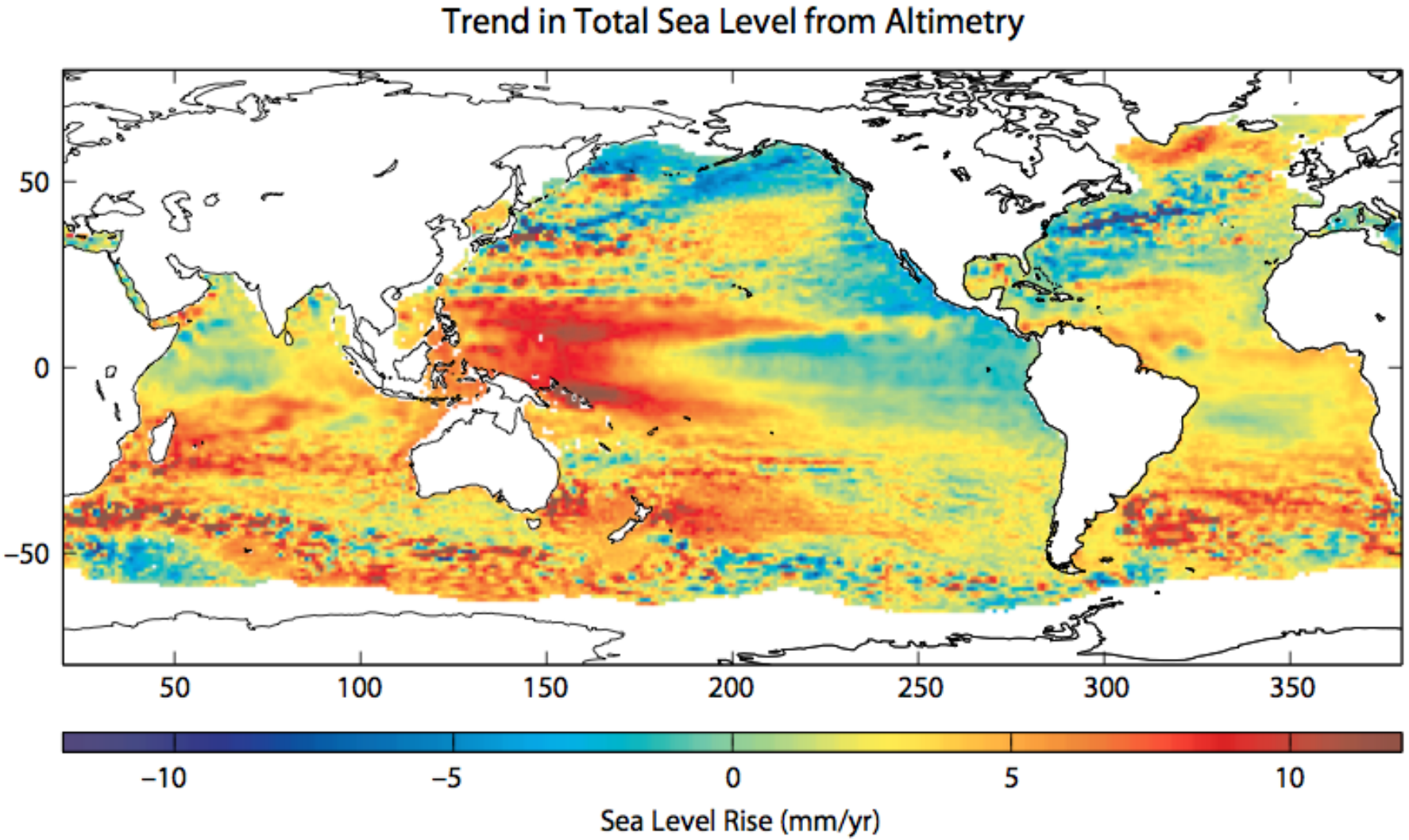

Figure 1. The regional change in sea level based on the 17-year trend from 1993 through 2009 from radar altimeter data from several satellites. Despite a fairly steady increase in globally averaged sea level rise (see Figure 2, inset), regional- scale changes over this duration are complicated and generally reflect changes in ocean circulation. Patterns reflecting other geophysical impacts, such as the net input of freshwater and changes in the gravity field due to loss of land ice, are expected to become clearer as the record length increases.

Even over a 20-year period most of the changes are associated with circulation changes from decadal natural variability of the ocean-atmosphere system. (Willis *et al.*, 2010)

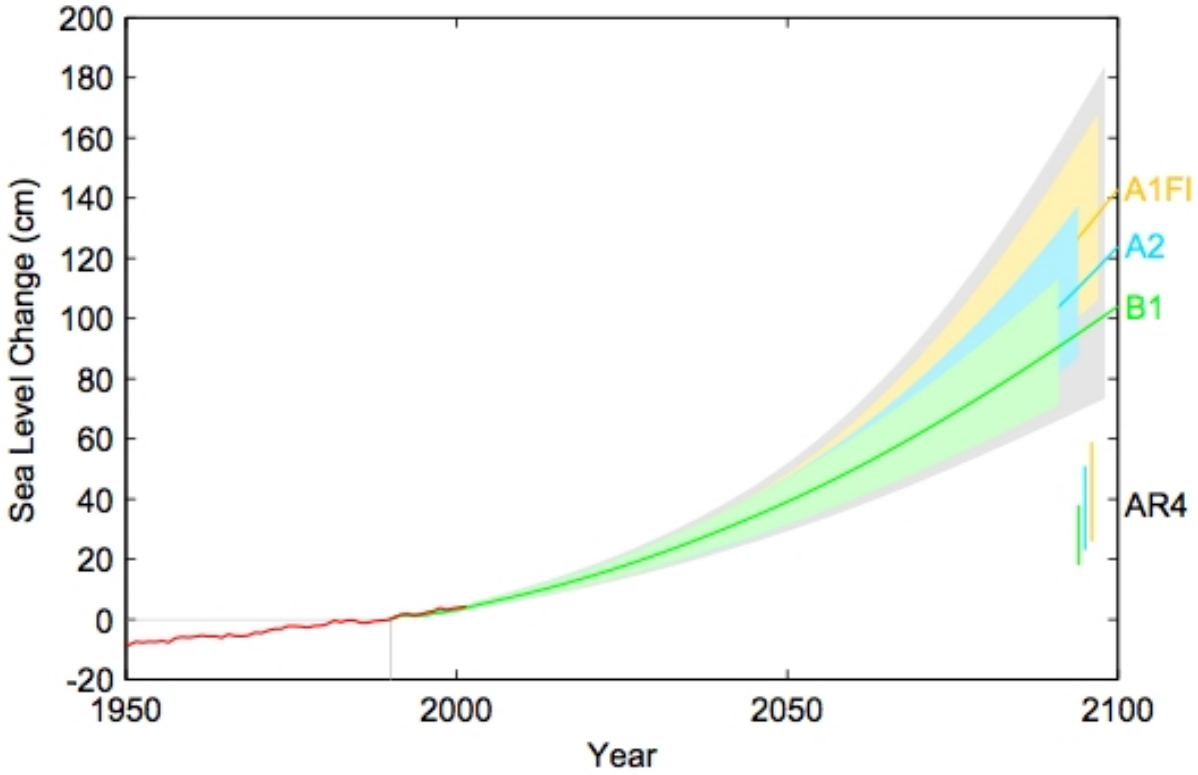

Fig. 6. Projection of sea-level rise from 1990 to 2100, based on IPCC temperature projections for three different emission scenarios (labeled on right, see Projections of Future Sea Level for explanation of uncertainty ranges). The sea-level range projected in the IPCC AR4 (2) for these scenarios is shown for comparison in the bars on the bottom right. Also shown is the observations-based annual global sea-level data (18) (red) including artificial reservoir correction (22).

An example of a recent revision of the expected sea level rise to be much higher (Vermeer and Rahmstorf, 2009). It is now widely agreed that IPCC (2007), $i.e.$, AR4, made a mistake by neglecting internal melting and flow of the major ice sheets and glaciers in Greenland and West Antarctica. Most recent estimates are for 0.5-2 m increase over the next century. The future is highly dependent on human emission behavior.

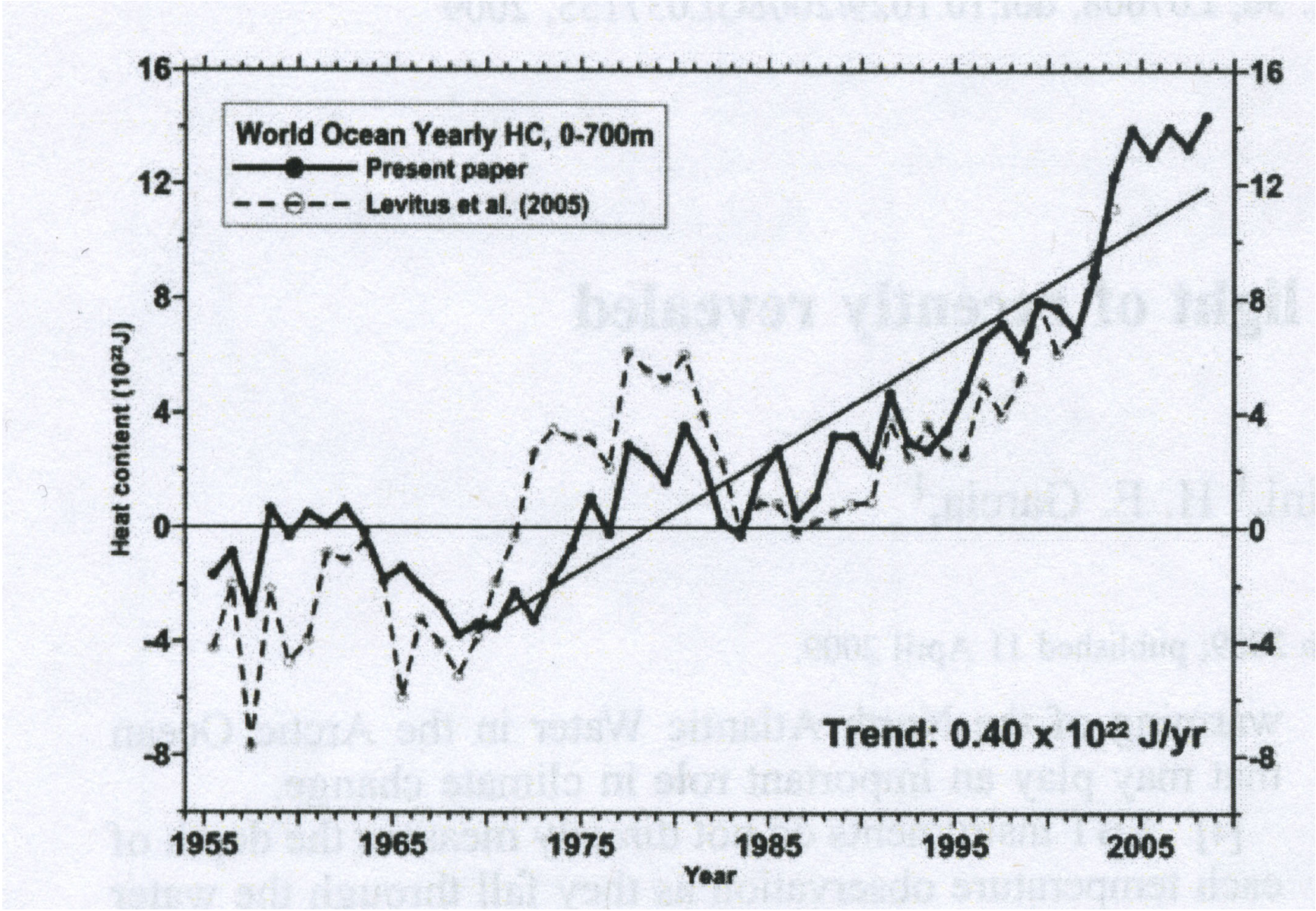

Time series of yearly ocean heat content (10^{22} J) for the 0-700 m layer from this study (solid) and from Levitus *et al.* (2005). The analysis differences are due to additional data and data corrections. There is net warming since around 1975-80. (Levitus *et al.*, 2009)

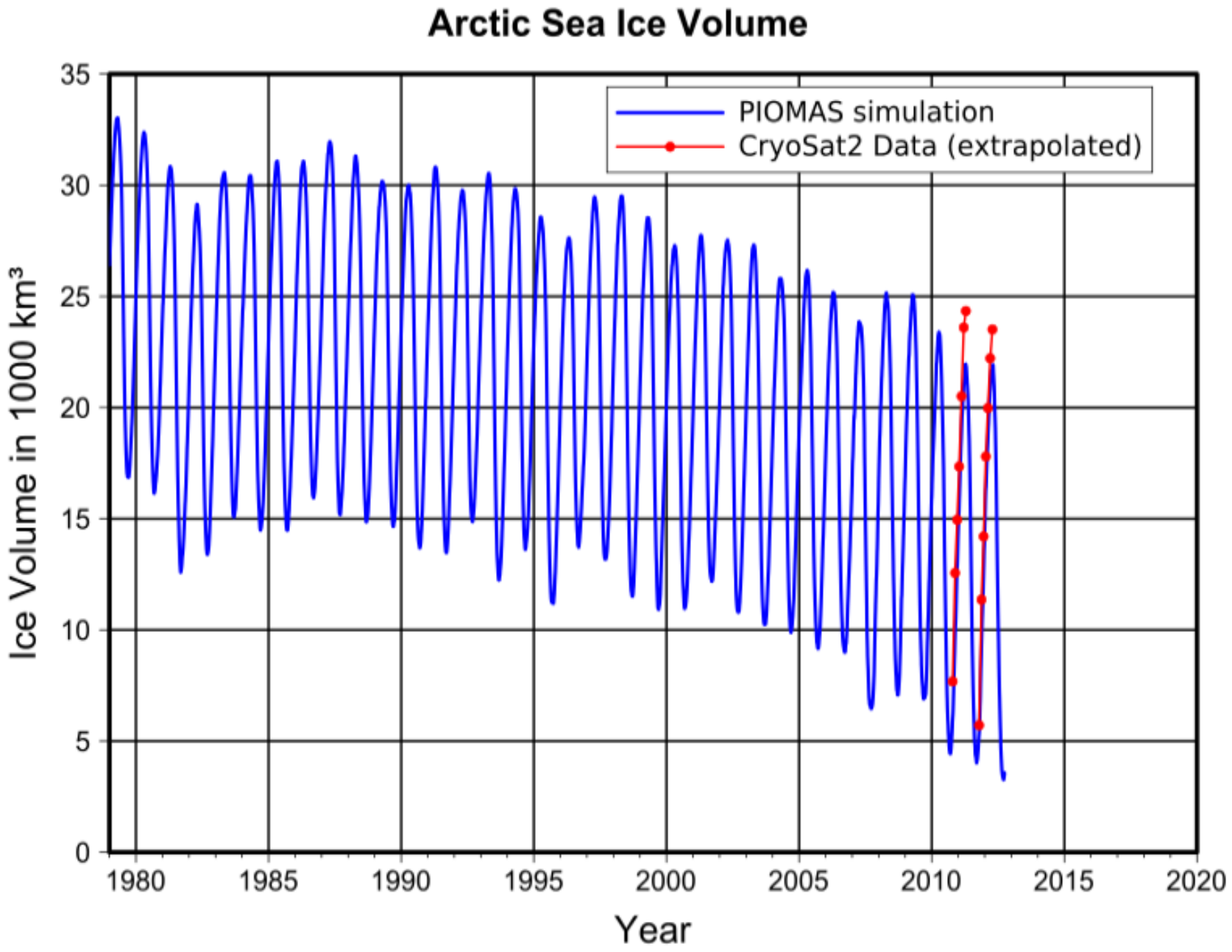

Arctic sea ice volume analyzed by the Pan-Arctic Ice-Ocean Modelling and Assimilation System (PIOMAS). The volume is rapidly declining, perhaps at an accelerating rate.

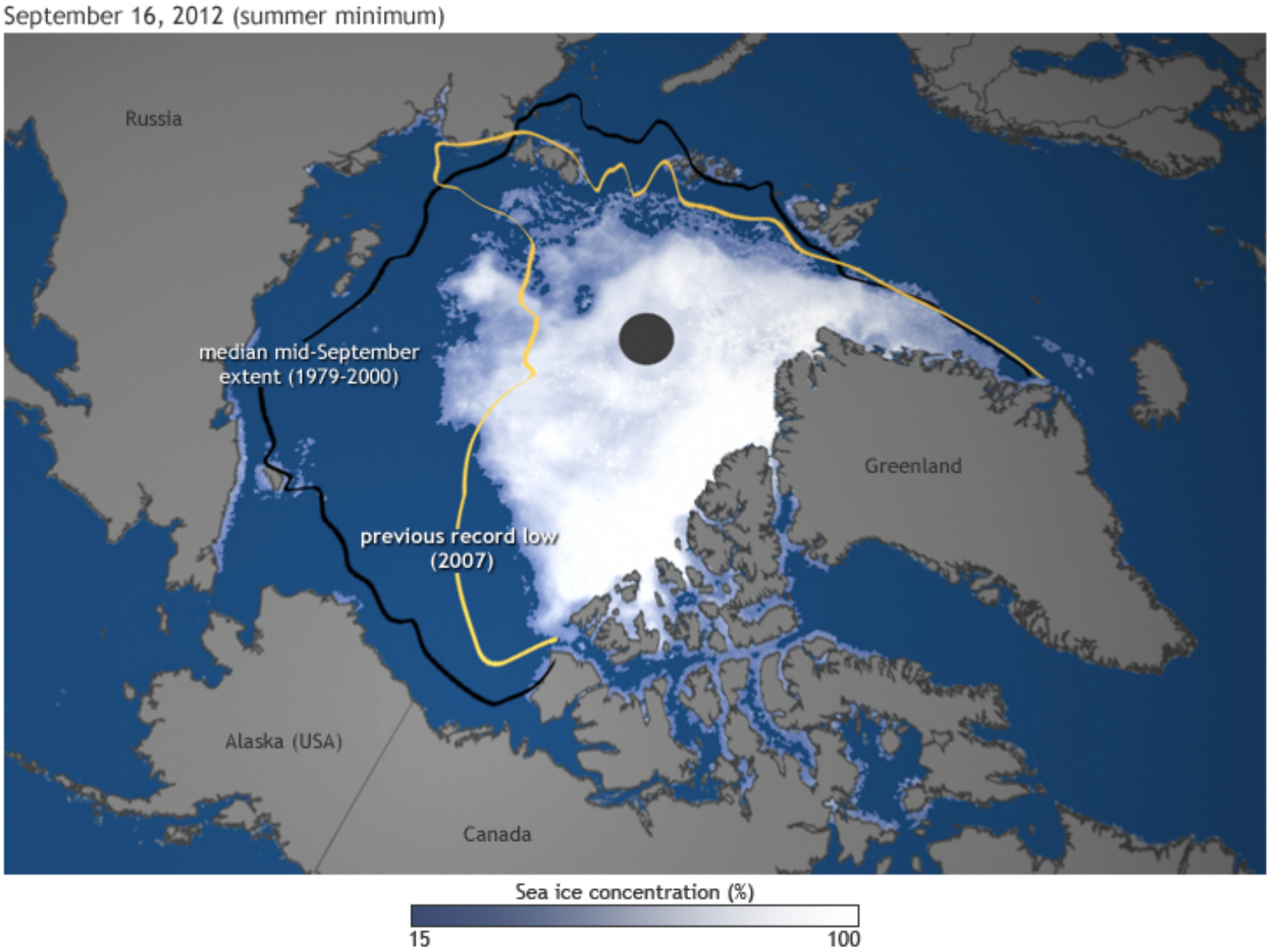

Map of Arctic sea ice at the time of its late-summer minimum. Depicted are the multi-decadal mean position, the anomalously small extent in 2007, and the even smaller extent in 2012. (Dan Pisuf, NOAA, based on data by from the National Snow and Ice Data Center)

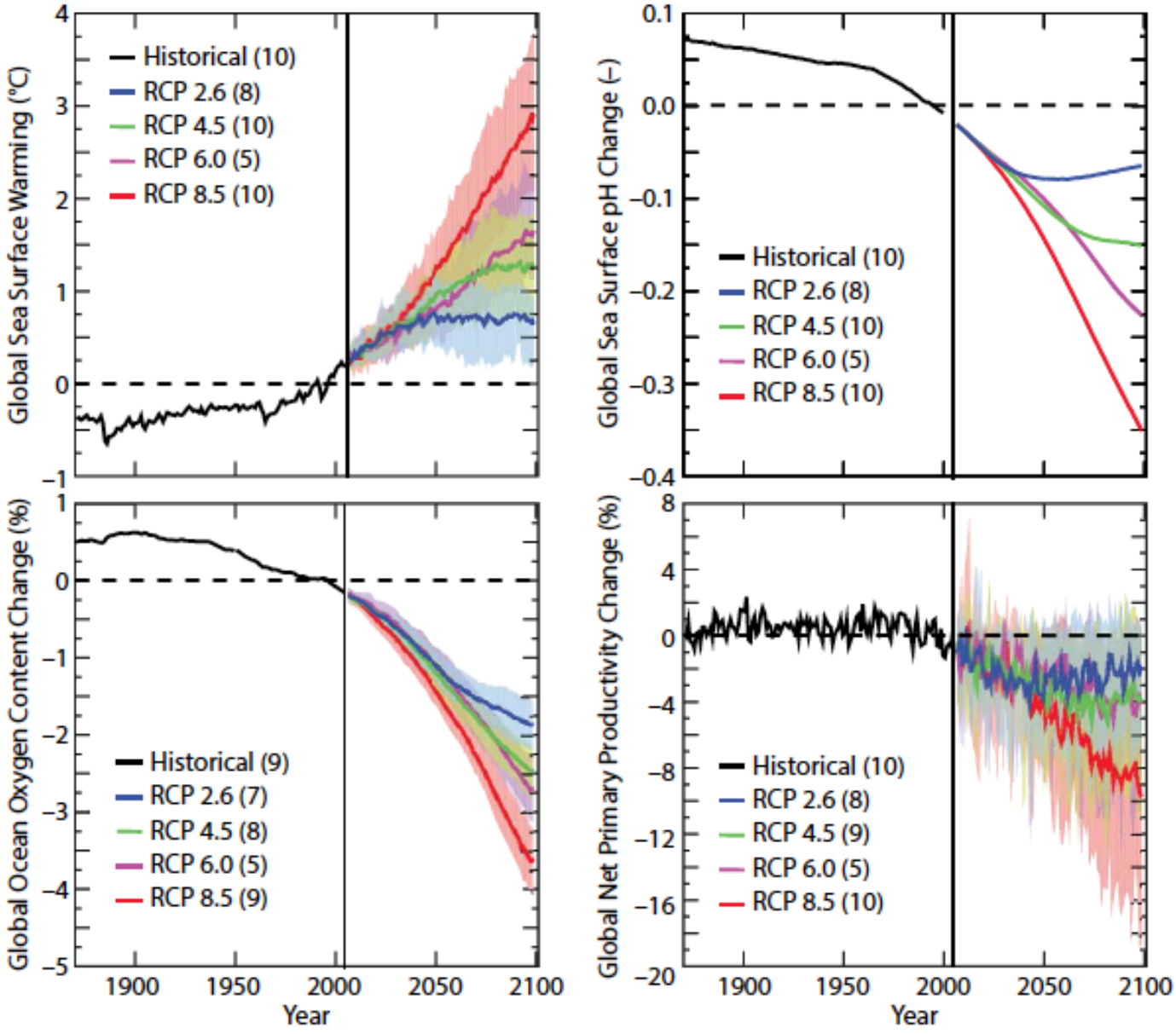

Figure 4. Time series of global average ocean anomalies for sea surface temperature (°C), surface pH, oxygen content (% change), and net primary productivity (% change) based on an ensemble-mean of Earth System Models (Bopp et al., 2013). The black lines represent model ensemble trends over the historical period and the colored lines future projections using four different emission scenarios or RCPs (Figure 2). The colored shadings are the model ensemble spread (inter-model standard deviation).

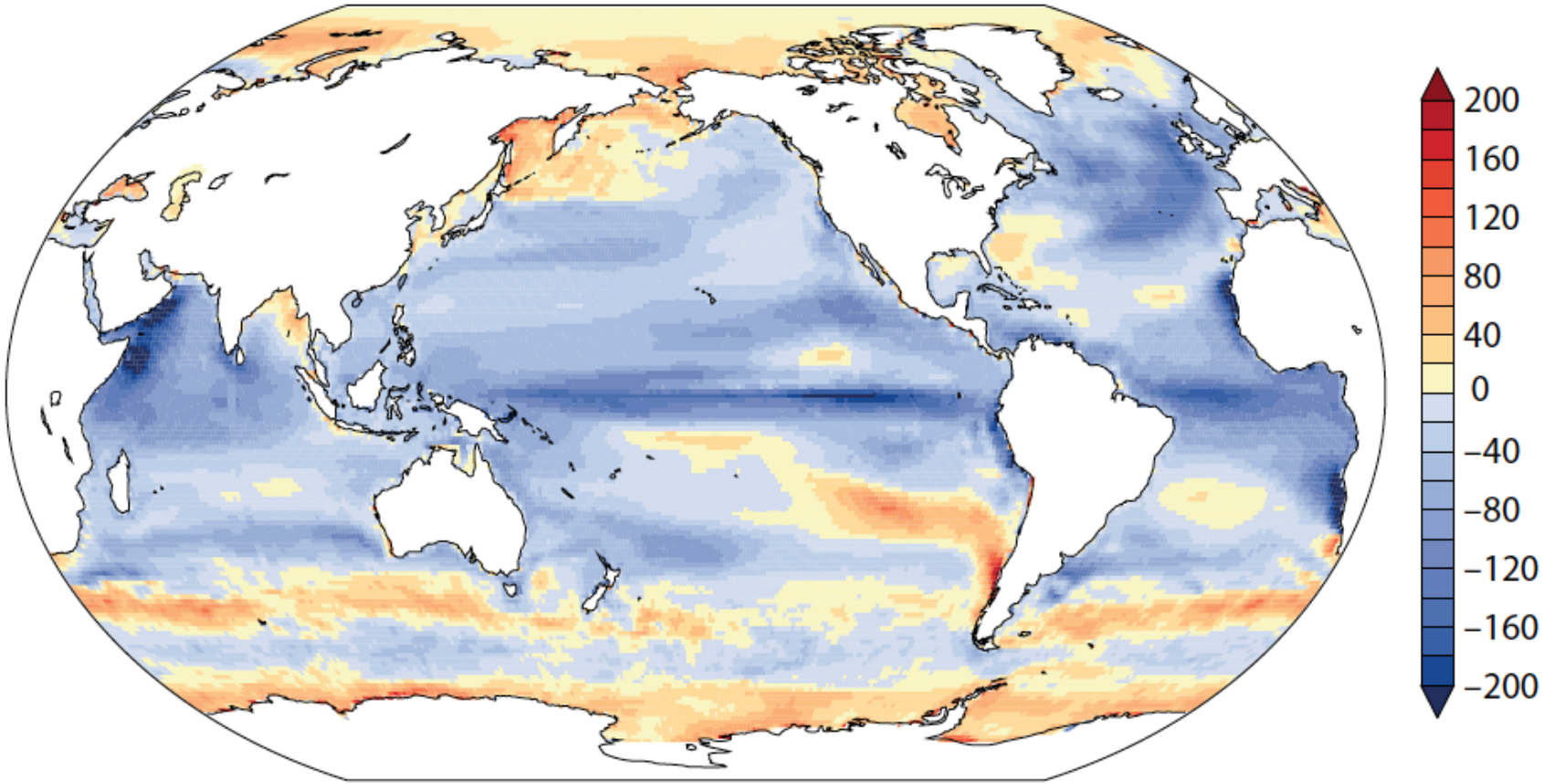

Figure 5. Spatial map of the change in marine net primary productivity (g C m^{-2} yr^{-1}; end of twenty-first century minus current conditions) based on the mean of an ensemble of 10 different CMIP5 models integrated in time following the RCP8.5 scenario (Figures 2 and 4) (Bopp et al., 2013).

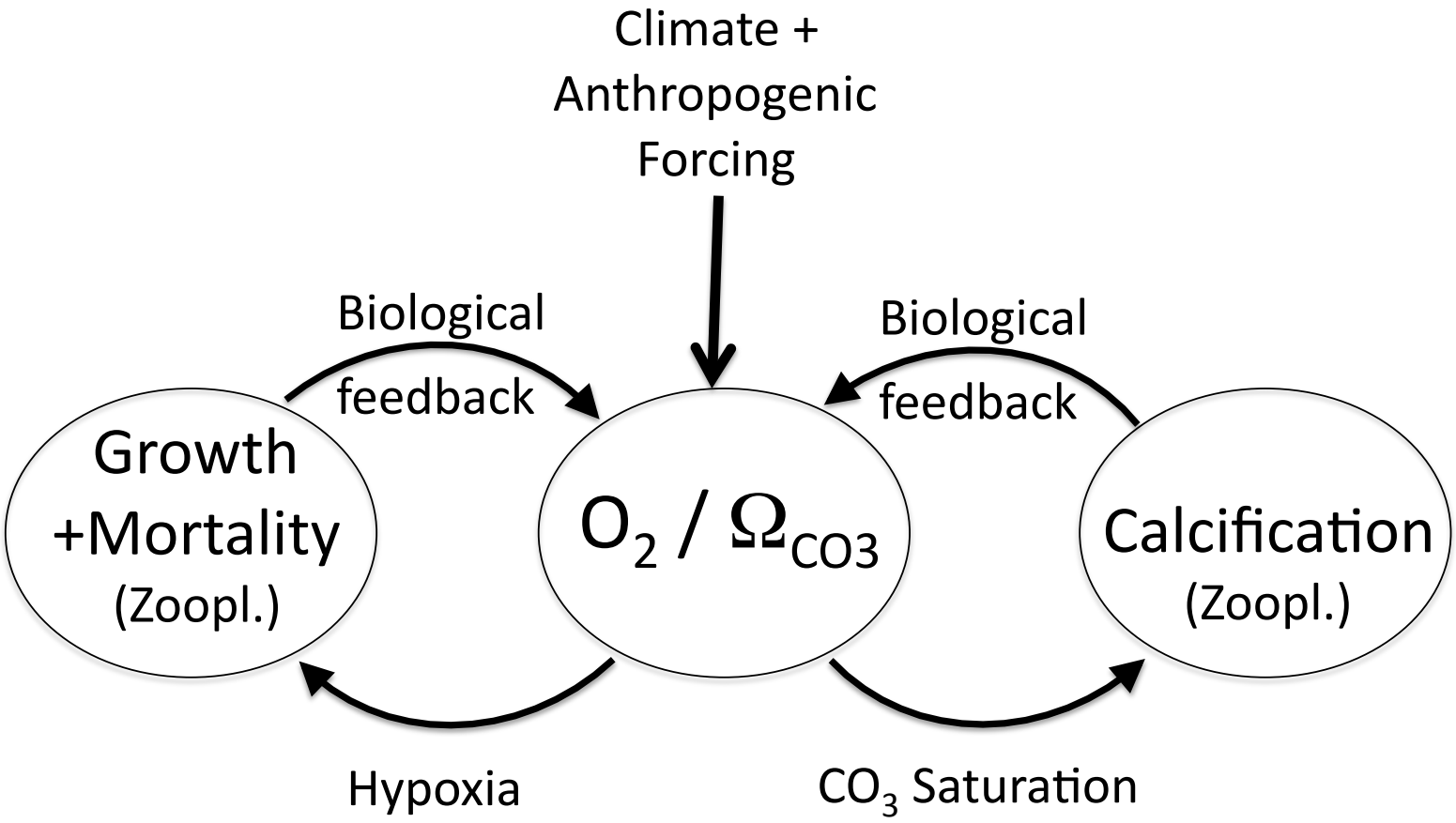

Conceptual model of biogeochemical feedbacks on ocean hypoxia and acidification. Climate forcing (e.g. warming and stratification) and anthropogenic inputs (e.g. nutrients and CO2) cause a reduction in O2 and carbonate saturation (Ω_{CO3}). These chemical perturbations cause a reduction in metabolically viable habitat and calcification rate for zooplankton. The reduced rates of growth and mineralization may feed back on the initial chemical change. The sign of the feedback will depend on vertical shifts in zooplankton activity within the water column.

Global change: stratification, hypoxia, acidification

RCP8.5: 2090-2099

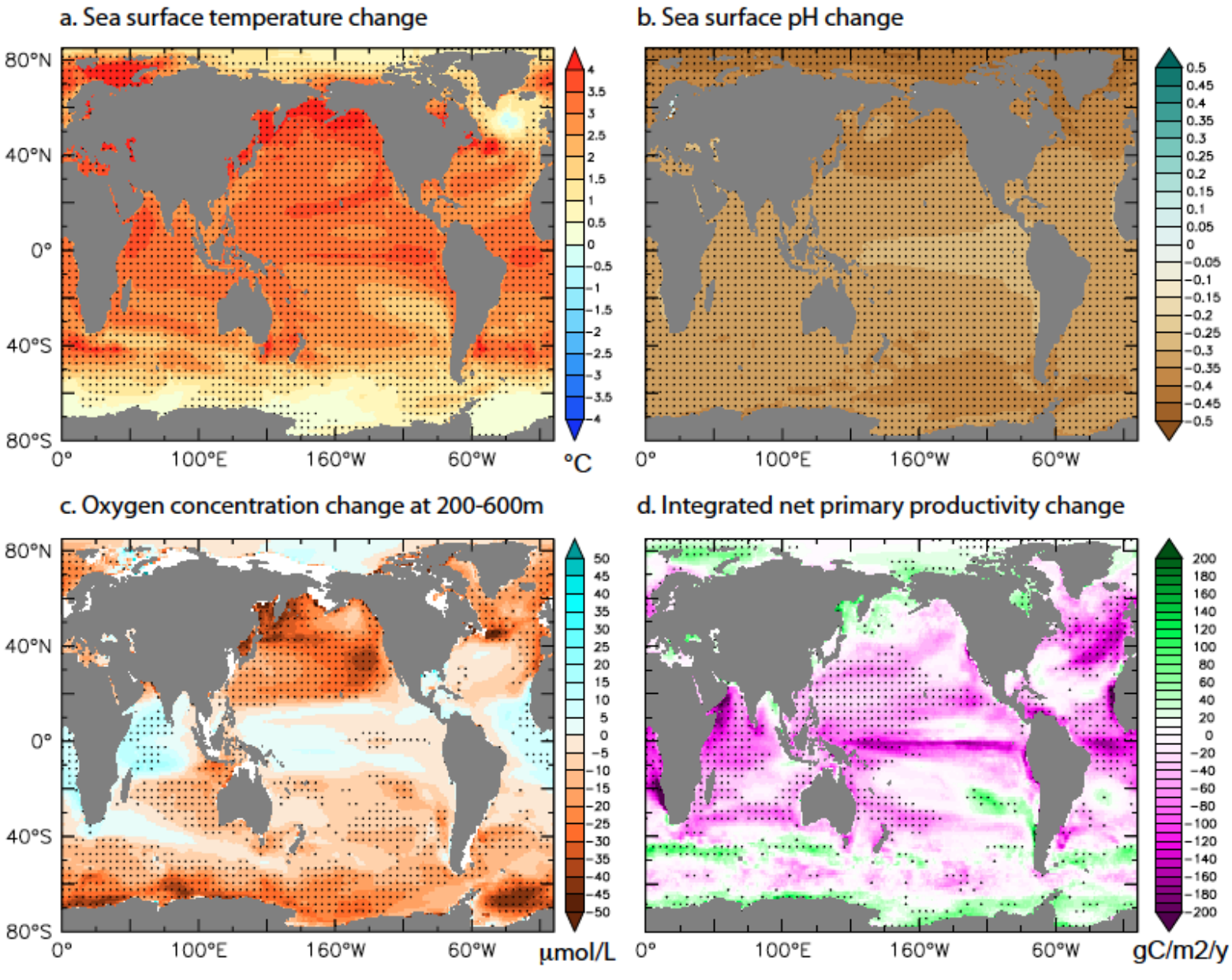

Bopp et al (2013)

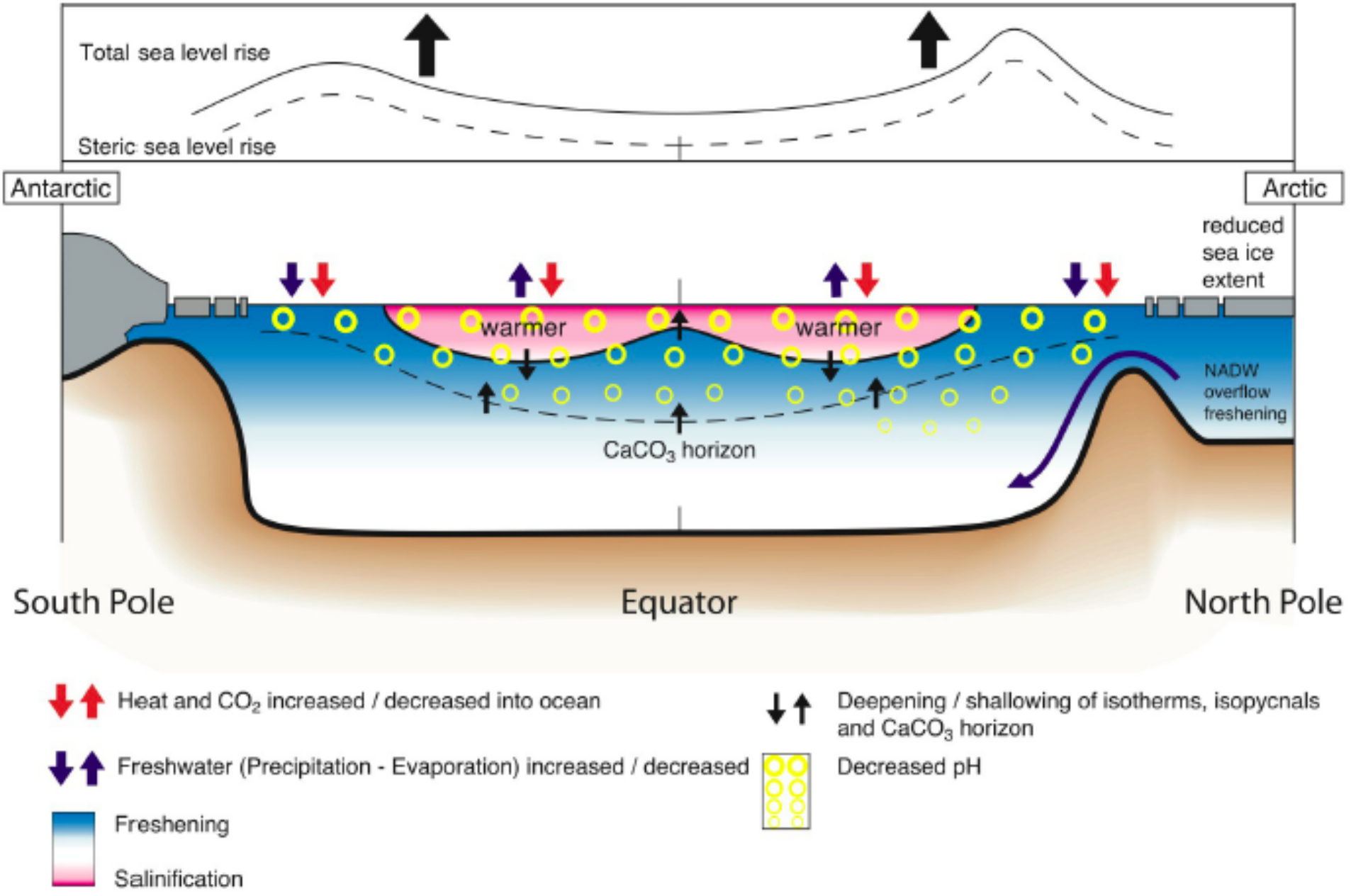

Summary of observed and expected anthropogenic climate changes in material distributions. (IPCC, 2007)

References

Bopp, L. *et al.*, 2013: Multiple stressors of ocean ecosystems in the 21^{st} century. *Biogeosciences* **10**, 225-245.

Curry, W., and D. Oppo, 2005: Glacial water mass geometry and the distribution of δ13C and ΣCO2 in the western Atlantic Ocean. *Paleoceanography* **20**, PA1017.

de Boyer Montegut, C., G. Madec, A. S. Fischer, A. Lazar, and D. Iudicone, 2004: Mixed layer depth over the global ocean: An examination of profile data and a profile-based climatology. *J. Geophys. Res.* **109**, C12003, doi:10.1029/2004JC002378.

Deutsch, C., S. Emerson, and L. Thompson, 2005: Fingerprints of climate change in North Pacific oxygen. *Geophys. Res. Lett.* **32**, L16604.

Galbraith, E., M. Kienast, S. Jaccard, T. Pedersen, B. Brunelle, D. Sigman, and T. Kiefer, 2008: Consistent relationship between global climate and surface nitrate utilization in the western subarctic Pacific throughout the last 500 ka. *Paleoceanography* **23**, PA2212.

Hall, A., and M. Visbeck, 2002: Synchronous variability in the Southern Hemisphere atmosphere, sea ice, and ocean resulting from the Annular Mode. *J. Climate* **15**, 3043-3057.

Hasselmann, K., 1976: Stochastic climate models. *Tellus* **28**, 473-485.

IPCC, 2007: *Climate Change 2007: The Physical Science Basis*, Chapter 5. Observations: Oceanic Climate Change and Sea Level, Fourth Assessment Report. Bindoff and Willebrand, coordinating lead authors.

Large, W. and S. Yeager, 2009: The global climatology of an interannually varying air-sea flux data set. *Climate Dyn.* **33**, 341-364.

Levitus, S., J. Antonov, T. Boyer, R. Locarnini, H. Garcia, and A. Mishonov, 2009: Global ocean heat content 1995-2008 in light of recently revealed instrumentation problems. *Geophys. Res. Lett.* **36**, L07608.

McManus, J., R. Francois, J.-M. Gheradi, L.D. Kelgwin, and S. Brown-Ledger, 2004: Collapse and rapid resumption of Atlantic meridional circulation linked to deglacial climate changes. *Nature* **428**, 834-837.

.

McPhadden, M., and D. Zhang, 2002: Slowdown of the meridional overturning circulation in the upper Pacific Ocean. *Nature* **415**, 603-608.

McWilliams, J.C., 2007: Irreducible imprecision in atmospheric and oceanic simulations. *Proc. Nat. Acad. Sci.* **104**, 8709-8713.

Mikaloff Fletcher, S., *et al.*, 2006: Inverse estimates of anthropogenic CO2 uptake, transport, and storage by the ocean. *Global Biogeochemical Cycles* **20**, GB2002.

Sabine, C.L., R.A. Feely, N. Gruber, R.M. Key, K. Lee, J.L. Bullister, R. Wanninkhof, C.S. Wong, D.W.R. Wallace, B. Tilbrook, F.J. Millero, T.H. Peng, A. Kozyr, T. Ono, and A.F. Rios, 2004: The oceanic sink for anthropogenic CO_2. *Science* **305**, 367-371.

Vermeer, M., and S. Rahmstorf, 2009: Global sea level linked to global temperature. *Proc. Nat. Acad. Sci.* **106**, 21527-21532.

Willis, J.K., D.P. Chambers, C.Y. Kuo, and C.K. Shum, 2010: Global sea level rise: recent progress and challenges for the decade to come. *Oceanography* **23**(4), 26-35.